Geochemistry Geophysics Geosystems G3
AN ELECTRONIC JOURNAL OF THE EARTH SCIENCES
Published by AGU and the Geochemical Society

Article
Volume 4, Number 6
28 June 2003
8711, doi:10.1029/2002GC000322
ISSN: 1525-2027

Trace element abundances of Mauna Kea basalt from phase 2 of the Hawaii Scientific Drilling Project: Petrogenetic implications of correlations with major element content and isotopic ratios

S. Huang and F. A. Frey

Department of Earth, Atmospheric and Planetary Sciences, Massachusetts Institute of Technology, Cambridge, MA 02139, U.S.A. (huangs@mit.edu; fafrey@mit.edu)

[1] The temporal geochemical variations defined by lavas erupted throughout the growth of a single volcano provide important information for understanding how the Hawaiian plume works. The Hawaii Scientific Drilling Project (HSDP) sampled the shield of Mauna Kea volcano to a depth of 3100 meters below sea level during Phase 2 of the HSDP. Incompatible element abundance ratios, such as La/Yb, Sm/Yb, Nb/Zr, and Ti/Zr, in conjunction with SiO_2 abundance and radiogenic isotopic ratios, especially He and Pb, in the reference sample suites of the Mauna Kea portion of cores from Phases 1 and 2 of the HSDP define three distinct geochemical groups. The upper 550 m of Mauna Kea lavas in the Phase 2 core include the Postshield Group with eruption ages of ~200 ka to <370 ka. These lavas have relatively low SiO_2 content, $^{3}He/^{4}He$ and $^{206}Pb/^{204}Pb$, and they define a trend to relatively high La/Yb, Sm/Yb, and Nb/Zr. The eruption of these lavas coincides with migration of the Mauna Kea shield off the hot spot. As a result, extent of melting decreased, melt segregation occurred at greater depth, within the garnet stability field, and a geochemically distinct component associated with the periphery of the plume was sampled. Deeper in the Phase 2 core two other geochemical groups of lava are intercalated. One group has relatively low SiO_2 abundance and high Nb/Zr Ti/Zr, $^{3}He/^{4}He$ and high $^{208}Pb/^{204}Pb$ at a given $^{206}Pb/^{204}Pb$. These are distinctive geochemical characteristics of lavas erupted at Loihi seamount. Variations in incompatible element abundance ratios (e.g., Sm/Yb versus Nb/Zr and La/Yb versus Ti/Zr) define mixing trends between these low SiO_2 lavas (Loihi-type) and lavas belonging to a high SiO_2 group that are the dominant lava type in the shield part of the core (Kea-type). These two groups are presumed to reflect components intrinsic to the plume. Correlations of incompatible element abundance ratios, such as La/Nb, with radiogenic isotope ratios show that Hawaiian shields contain different proportions of geochemically distinctive components. The Koolau shield contains a recycled sedimentary component that is not present in the Mauna Kea shield. The anomalously high Ba/Th in Hawaiian lavas is inferred to be a source characteristic. Ba/Th is correlated with some radiogenic isotope ratios in Kilauea and Mauna Loa lavas, but there is no correlation in Mauna Kea lavas which range in Ba/Th by a factor of 2.6.

Components: 21,976 words, 21 figures, 7 tables.

Keywords: Hawaii Scientific Drilling Project; trace element; Hawaiian plume; Mauna Kea Volcano.

Index Terms: 1010 Geochemistry: Chemical evolution; 1025 Geochemistry: Composition of the mantle; 1065 Geochemistry: Trace elements (3670); 3670 Mineralogy, Petrology, and Mineral Physics: Minor and trace element composition.

Received 30 January 2002; **Revised** 18 December 2002; **Accepted** 31 January 2003; **Published** 28 June 2003.

Huang, S., and F. A. Frey, Trace element abundances of Mauna Kea basalt from phase 2 of the Hawaii Scientific Drilling Project: Petrogenetic implications of correlations with major element content and isotopic ratios, *Geochem. Geophys. Geosyst.*, *4*(6), 8711, doi:10.1029/2002GC000322, 2003.

Theme: Hawaii Scientific Drilling Project **Guest Editors:** Don DePaolo, Ed Stolper, and Don Thomas

1. Introduction

[2] In order to understand processes occurring within the earth's mantle, it is necessary to determine the role of mantle plumes in creating ocean island volcanoes. The strongest evidence for long-lived mantle plumes arises from volcanic chains that define age progressive hot spot tracks; the Hawaiian Ridge and Emperor Seamount Chain are well documented examples. An important approach for determining how a plume "works" is to study the life history of a single volcano as it approaches, passes over and moves away from the hot spot. This is a principal objective of the Hawaiian Scientific Drilling Project (HSDP) which is focused on sampling a large portion of the growth of Mauna Kea Volcano [*Stolper et al.*, 1996].

[3] Core from the pilot hole of HSDP (designated Phase 1 in following text) drilled near Hilo, Hawaii recovered 280 m of lavas derived from Mauna Loa Volcano overlying 776 m of subaerially erupted Mauna Kea lavas ranging in age from <200 ka to ~400 ka [*Sharp et al.*, 1996]. Based on the success of this Phase 1 hole, Phase 2 of HSDP drilled and cored (95% recovery) Mauna Loa and Mauna Kea shield lavas to a depth of 3098 meters below sea level (mbsl) at a site ~2 km south of the Phase I hole [*DePaolo et al.*, 1999]. From top to bottom this core includes 246 m of subaerially erupted Mauna Loa lavas, 833 m (~120 flow units) of subaerially erupted Mauna Kea lavas which at the depth of 1079 mbsl abruptly change to 905 m of submarine lavas, dominantly basaltic hyaloclastite debris flows but with a significant proportion of massive basalt with relatively low vesicularity. The lowermost 1114 m of Phase 2 core is ~60% pillow lavas intercalated with volcaniclastic sediment. Also thirteen intrusive units occur in the deepest parts of the core forming ~7% of the core from 2500 to 3100 mbsl. Both cores are dominantly tholeiitic basalt, but alkalic basalt occurs in the uppermost parts of the Mauna Kea section in both the Phase 1 (nine flow units [*Yang et al.*, 1996]) and Phase 2 cores (two flow units (J. M. Rhodes and M. Vollinger, Geochemical stratigraphy of basaltic lavas from HSDP 2, manuscript submitted to *Geochemistry Geophysical Geosystems*, 2002, hereinafter referred to as Rhodes and Vollinger, submitted manuscript, 2002)). Eruption ages for Mauna Kea lavas in the Phase 2 core range from <230 ka to 630 ka (all ages mentioned in this text are measured, interpolated or extrapolated data from W. Sharp et al., The $^{40}Ar/^{39}Ar$ dating of lavas, hyaloclastics, and intrusions from HSDP 2 core, manuscript submitted to *Geochemistry Geophysics Geosystems*, 2002).

[4] Our research effort is part of a team effort to determine and interpret temporal geochemical variations of lavas forming the shield of Mauna Kea Volcano. We have determined abundances of trace elements in the reference suite of samples [*DePaolo et al.*, 1999] from the Mauna Kea portion of the Phase 2 core (100 samples) by instrumental neutron activation (INAA) and inductively coupled plasma mass spectrometry (ICP-MS) (Table 1). We analyzed aliquots of the reference suite powders prepared by Rhodes and Vollinger (submitted manuscript, 2002). Details of the analytical procedures, estimates of accuracy and precision are discussed in Appendix A. Many trace elements were analyzed by ICP-MS, INAA and XRF (Rhodes and Vollinger, submitted manuscript, 2002), and the comparisons of the three data sets are in Appendix A. Figures in this paper show ICP-MS data unless noted otherwise in the figure captions. Our objective is to use these data along with major and trace element abundances determined by X-ray fluorescence (XRF) (Rhodes and Vollinger, submitted manuscript, 2002) and radiogenic isotopic ratios (J. Blichert-Toft et al., High resolution and high precision Hf and Pb

Table 1 (Representative Sample). Trace Element Abundances in Mauna Kea Lavas Recovered From HSDP Phase 2 Drill Hole[a] [The full Table 1 is available in the HTML version of this article at http://www.g-cubed.org.]

	SR0121 −4.40	SR0124 −3.90	SR0125 −6.25	SR0127 −4.75	SR0129 −5.20	SR0131 −6.92	SR0133 −8.20	SR0137 −5.98	SR0141 −7.90	SR0148 −8.50	SR0157 −6.25	SR0167 −5.90	SR0175 −5.25	SR0184 −2.80	SR0193 −0.00	SR0205 −1.30	SR0212 −8.20
Depth (mbsl)	246.2	252.9	256.5	261.7	267.5	274.4	281.3	293.0	305.8	326.7	353	378.4	398.1	421.2	443.6	467.8	490.9
Rock Type	subaerial	subaerial	subaerial	subaerial	subaerial	subaerial	subaerial	subaerial	subaerial	subaerial	subaerial	subaerial	subaerial	subaerial	subaerial	subaerial	subaerial
UNIT	U0042	U0043	U0045	U0046	U0047	U0048	U0049	U0053	U0056	U0060	U0065	U0070	U0073	U0076	U0080	U0083	U0088
ICP-MS																	
Rb	13.0	1.68	1.96	9.72	1.36	14.0	5.03	3.40	3.48	0.531	3.16	1.38	0.356	4.40	6.51	4.88	3.78
Sr	470	414	318	462	496	604	364	389	416	211	213	375	151	228	297	268	238
Y	39.5	35.6	29.8	31.3	29.2	38.9	26.2	30.8	34.1	18.1	18.5	32.8	14.2	21.0	26.0	22.3	20.7
Zr	248	234	195	198	162	293	168	188	210	102	101	193	75.3	122	152	131	116
Nb	28.4	23.0	20.1	19.4	14.9	29.4	15.9	16.1	19.8	8.71	8.05	16.5	6.13	9.28	13.0	11.9	9.60
Ba	317	204	181	173	155	248	134	137	166	62.9	68.7	137	52.5	78.0	107	91.9	80.6
La	24.8	19.9	18.7	16.8	13.1	24.4	14.0	13.9	16.9	7.59	7.20	14.8	5.26	8.14	11.1	9.82	8.26
Ce	52.9	46.8	42.5	41.0	31.7	59.0	33.8	34.2	40.9	18.6	18.1	37.4	12.8	20.6	27.4	24.8	20.2
Pr	7.98	7.05	6.18	5.98	4.84	8.67	5.00	5.22	6.18	2.91	2.81	5.67	2.07	3.18	4.13	3.74	3.19
Nd	34.9	31.7	28.1	27.0	22.7	38.7	22.9	24.2	28.4	13.7	13.5	26.2	9.69	15.7	20.1	17.6	15.2
Sm	8.58	7.92	7.25	6.87	6.02	9.69	5.79	6.40	7.28	3.70	3.72	7.13	2.72	4.34	5.32	4.68	4.16
Eu	2.89	2.64	2.33	2.25	2.13	3.15	1.90	2.21	2.48	1.24	1.24	2.31	0.935	1.44	1.83	1.58	1.44
Gd	8.60	8.09	7.15	6.94	6.22	9.66	5.80	6.54	7.52	3.85	3.82	7.27	3.00	4.35	5.40	4.91	4.35
Tb	1.33	1.27	1.12	1.09	1.00	1.48	0.919	1.05	1.19	0.621	0.615	1.14	0.471	0.717	0.914	0.770	0.710
Dy	6.97	6.66	5.88	5.92	5.48	7.66	4.91	5.80	6.46	3.43	3.42	6.31	2.67	3.97	4.94	4.25	3.93
Ho	1.37	1.28	1.07	1.12	1.04	1.42	0.911	1.12	1.25	0.64	0.685	1.20	0.518	0.769	0.957	0.798	0.773
Er	3.27	3.20	2.57	2.75	2.58	3.35	2.23	2.68	3.03	1.60	1.70	2.90	1.30	1.83	2.29	2.00	1.90
Tm	0.445	0.424	0.364	0.440	0.351	0.458	0.312	0.379	0.415	0.222	0.224	0.393	0.177	0.265	0.334	0.279	0.257
Yb	2.63	2.43	2.06	2.22	2.01	2.64	1.80	2.18	2.45	1.30	1.38	2.33	1.01	1.53	1.86	1.62	1.55
Lu	0.355	0.333	0.292	0.300	0.280	0.358	0.245	0.303	0.334	0.175	0.190	0.323	0.145	0.212	0.260	0.222	0.219
Hf	6.19	5.94	4.92	4.94	4.22	7.06	4.14	4.59	5.35	2.57	2.69	5.07	1.95	3.07	3.78	3.37	3.01
Ta[b]	1.86	1.57	1.28	1.31	1.01	2.01	1.11	1.14	1.37	0.664	0.673	1.16	0.576	0.735	0.980	0.916	0.800
Pb	1.51	1.38	1.28	1.22	0.989	1.61	0.962	1.00	1.17	0.91	0.593	1.18	0.484	0.649	0.787	0.820	0.665
Th	1.71	1.49	1.44	1.36	0.945	1.97	1.06	0.994	1.24	0.526	0.542	1.14	0.382	0.607	0.858	0.801	0.597
U	0.471	0.440	0.382	0.409	0.202	0.610	0.286	0.285	0.300	0.152	0.192	0.260	0.0976	0.188	0.270	0.252	0.201
INAA																	
Na_2O	2.05	1.83	1.29	2.35	2.21	2.81	1.81	2.03	2.35	1.07	1.25	2.11	0.88	1.35	1.88	1.4	1.51
Cr	140	328	609	182	271	129	839	454	214	1830	1268	349	1660	1209	592	1038	1204
Sc	29.3	29.2	35.9	29.8	29.8	25.8	25.9	30.5	30.1	22.5	22.1	27.8	17	21.9	28.7	22.1	25.7
La	22.8	18.6	18.7	16.4	12.9	23.6	13.9	13.8	16.4	7.39	6.92	13.7	4.85	7.41	11	8.96	8.08
Ce	51.7	45.8	44.3	42	33.4	59.9	35	36.2	43.1	18.6	18.4	35.3	12.3	19.4	28	23.5	20.8
Nd	32.9	30.7	30.3	27.8	23	39.1	23.1	23.2	28.2	13.8	11.8	24.2	8.8	13.5	19.3	15.9	16.1
Sm	7.92	7.65	7.24	6.7	6.02	9.3	5.66	6.34	7.13	3.46	3.44	6.42	2.53	3.81	5.16	4.21	4.08

[a] Trace element abundances were determined by ICP-MS and INAA separately, and are reported in ppm, except for Na_2O which is reported in %. n.d., not determined. For discussion of accuracy and precision see Appendix A.

[b] Samples were powdered in WC shatterbox [*Rhodes and Vollinger*, 2002]; therefore, the Ta contents may be anomalously high. However, this effect appears to be minor (see text and Figure 12c).

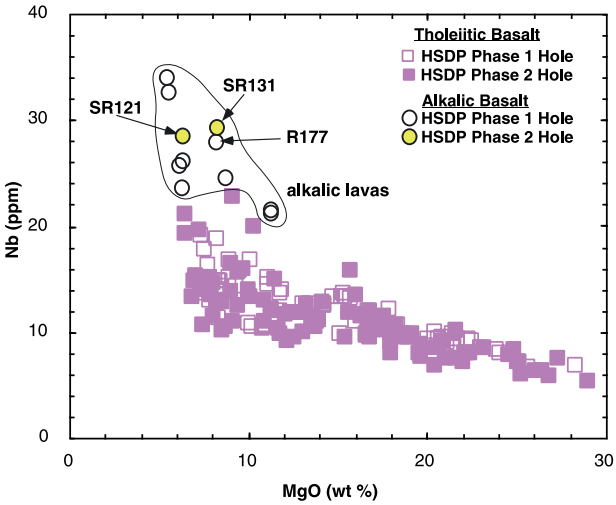

Figure 1. Nb abundance (ppm) versus MgO content (wt.%) showing that Nb abundance is inversely correlated with MgO content in tholeiitic basalt from the Phase 1 and 2 cores of the HSDP. The wide range in MgO and inverse trend reflects olivine accumulation and magma mixing (Rhodes and Vollinger, submitted manuscript, 2002). The eleven samples of alkalic basalt, (nine from Phase 1 hole, two, SR121 and SR131, from Phase 2 hole) however, are offset to higher Nb abundance at a given MgO content. In this and following figures, data are for the reference suites of HSDP samples [*Hawaii Scientific Drilling Project*, 1994; *DePaolo et al.*, 1999]. Data for MgO are from *Rhodes* [1996] for the Phase 1 hole and Rhodes and Vollinger (submitted manuscript, 2002) for the Phase 2 hole. Data for Nb are from *Rhodes* [1996] for the Phase 1 hole and this paper for the Phase 2 core.

isotope stratigraphy of Mauna Loa and Mauna Kea lavas from HSDP 2, manuscript submitted to *Geochemistry Geophysics Geosystems*, 2002; J. Bryce and D. DePaolo, High resolution Sr and Nd isotopic records of Mauna Kea volcano: Results from the second phase of Hawaii Scientific Drilling Project (HSDP 2), manuscript submitted to *Geochemistry Geophysics Geosystems*, 2002; M. D. Kurz et al., Helium isotope variations in HSDP lavas, manuscript submitted to *Geochemistry, Geophysics, Geosystems*, 2002) to understand how the geochemical characteristics of these lavas were affected by postmagmatic alteration, crystal fractionation within the crust, and mantle processes, such as extent of melting. To constrain the source components contributing to Hawaiian shield building lavas, we also evaluate correlations between abundance ratios of incompatible elements and radiogenic isotopic ratios in lavas from Mauna Kea and other Hawaiian shields.

2. Results: Incompatible Trace Elements

[5] Abundances of incompatible elements that are not very sensitive to postmagmatic alteration, such as Nb, are inversely correlated with MgO content. This correlation is not linear because at a given MgO content the alkalic basalts are offset to higher Nb content (Figure 1). Within the HSDP Phase 2 reference suite of samples, the abundance range of incompatible elements varies from ~3 for moderately incompatible elements such as heavy rare earth elements (REE) to ~5 to 8 for highly incompatible elements, such as Ba, Th, U, Nb and light REE (Figure 2a). Generally this is also the order of increasing variability in abundance as indicated by the percent standard deviation (Figure 2b). For most incompatible elements the highest abundances are in the two alkalic lavas, SR 121 and SR 131 (Table 1, Figure 3). Note that the complete sample identification numbers are given in Table 1, but for brevity in the text we identify each reference sample only by SR number for Phase 2 and R number for Phase 1.

[6] Based on compositional similarity, alkalic basalt SR 131 from the Phase 2 core is from the same flow as sample R 177 from the Phase 1 core (Table 2). Both R 177 and SR 131 have unusually low SiO_2 contents and high alkalinity; they define the extremes in their respective cores (see Figure 1a of *Yang et al.* [1996] and Figure 3 of Rhodes and Vollinger (submitted manuscript, 2002)), In addition these samples are from units with similar eruption ages of ~240 ka (Table 2).

[7] The systematic increase in abundance range from moderately to highly incompatible elements is consistent with control of incompatible element abundances (except Rb) by igneous processes involving mafic minerals such as olivine, pyroxenes, and perhaps garnet. Based on analyses of multiple samples from individual flow units in the Phase 2 core (Huang, Vollinger, Frey, and Rhodes, unpublished data, 2003), the extremely large range in Rb abundance (~40, Figure 2a inset) reflects the effects of postmagmatic processes whereas Nb and

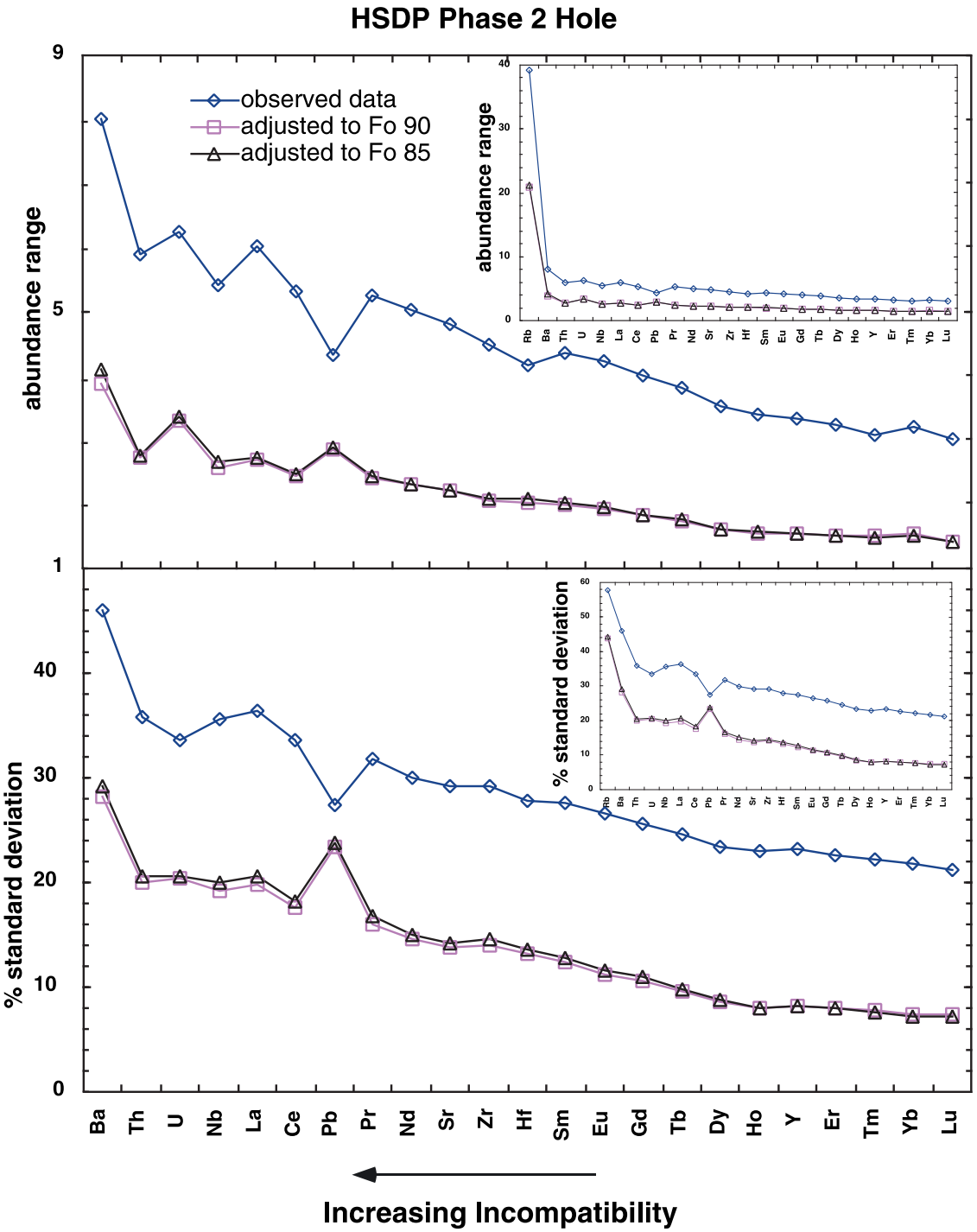

Figure 2. The abundance range (i.e., for each element the highest abundance in HSDP 2 samples is divided by the lowest abundance) and one standard deviation (in percent of the mean abundance) for reference suite samples from the Phase 2 HSDP core. Elements are arranged in order of incompatibility for peridotite/melt partitioning with the most incompatible elements on the left. Both the abundance range and percent standard deviation increase with increasing incompatibility (for unknown reasons Pb is an exception). As discussed later in the text much of the abundance variation arises from accumulation of olivine. Abundance variation for each incompatible element decreases significantly (assuming $D_x^{ol/melt} = 0$) after lava compositions are adjusted to be in equilibrium with a common olivine composition (Fo_{85} or Fo_{90}). In general, this adjustment decreases the the range and percent standard deviation by a factor of two. Insets show that Rb abundance is much more variable than abundances of other elements.

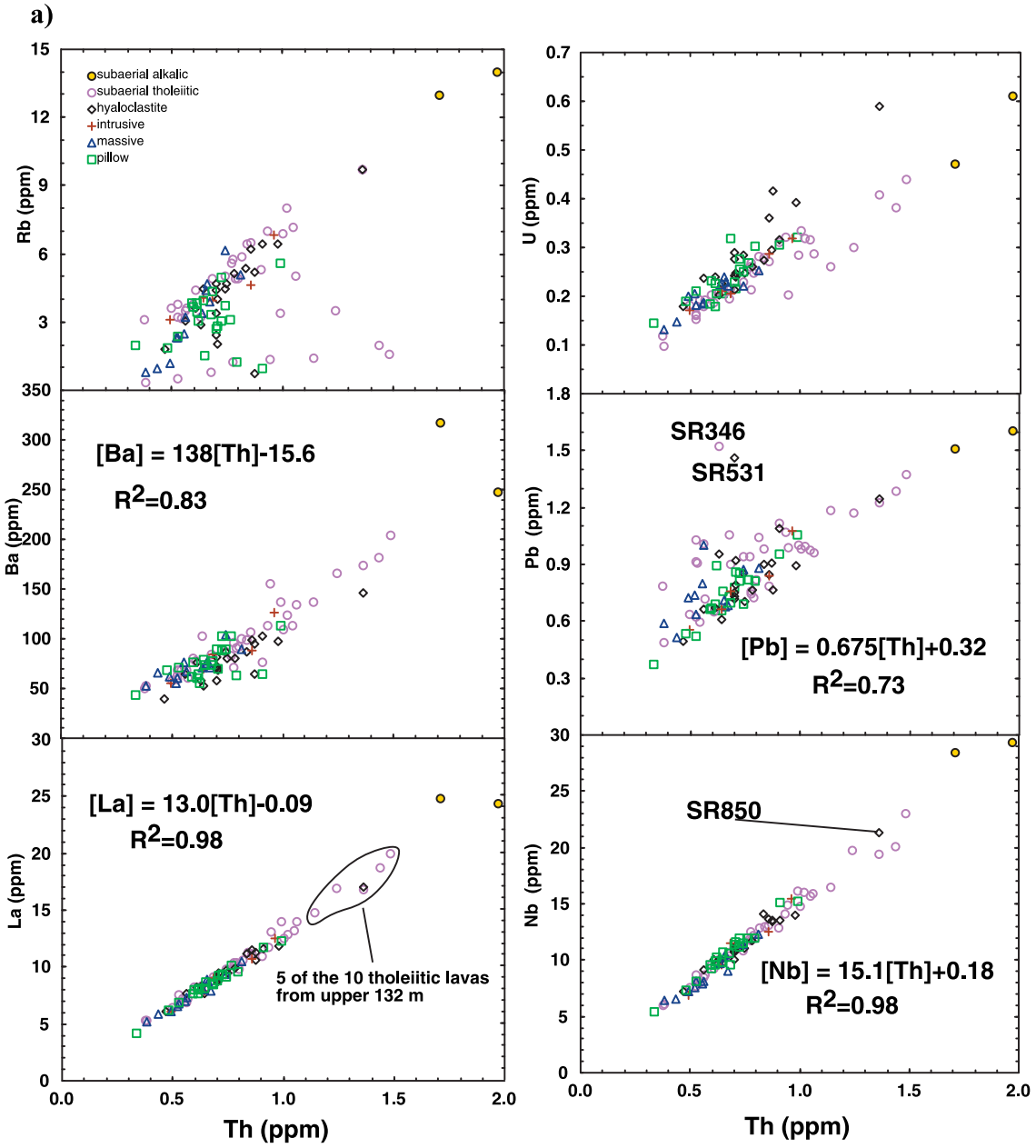

Figure 3. (a) Abundances of the highly incompatible elements Rb, U, Ba, Pb, La and Nb versus Th abundance (all in ppm) in basalt from the Phase 2 core. Th is the most incompatible element, i.e., the largest abundance range in Figure 2a, that was not mobile during postmagmatic alteration. The abundance trends for Rb and U are scattered because of their mobility during postmagmatic alterations. Ba and Pb are positively correlated with Th content but especially for Pb there is significant scatter. The correlation coefficient for Pb excludes the two labeled samples with anomalously high Pb content. These samples may have been contaminated with Pb (see Eisele et al. (submitted manuscript, 2002) for isotopic evidence for Pb contamination of subaerially erupted samples). Abundance of La and Nb are highly correlated with near zero intercepts, as indicated by equations for the best fit line. Data symbols indicate the various types of basalt samples recovered in the HSDP Phase 2 core. There is no correlation of composition with lava type (i.e., subaerial eruptive, pillow basalt, etc.), but the 7 samples with >l.1 ppm Th include the two samples of alkalic basalt and 5 of the 10 tholeiitic basalt lavas from the upper 132 m of the Mauna Kea section (circled in the La panel). In addition, SR 850, a low MgO (6.44%) tholeiitic basalt from deep in the core has high abundances of incompatible elements. (b) Abundances of the moderately incompatible elements, Sr, Sm, Hf, Y and Lu versus Th abundance (all in ppm). At less than ~1 ppm Th these trends are linear, but at higher Th abundance the trends become convex upwards indicating that if these samples are genetically related, the elements Sr, Sm, Zr, Hf, Y and Lu were more compatible than Th.

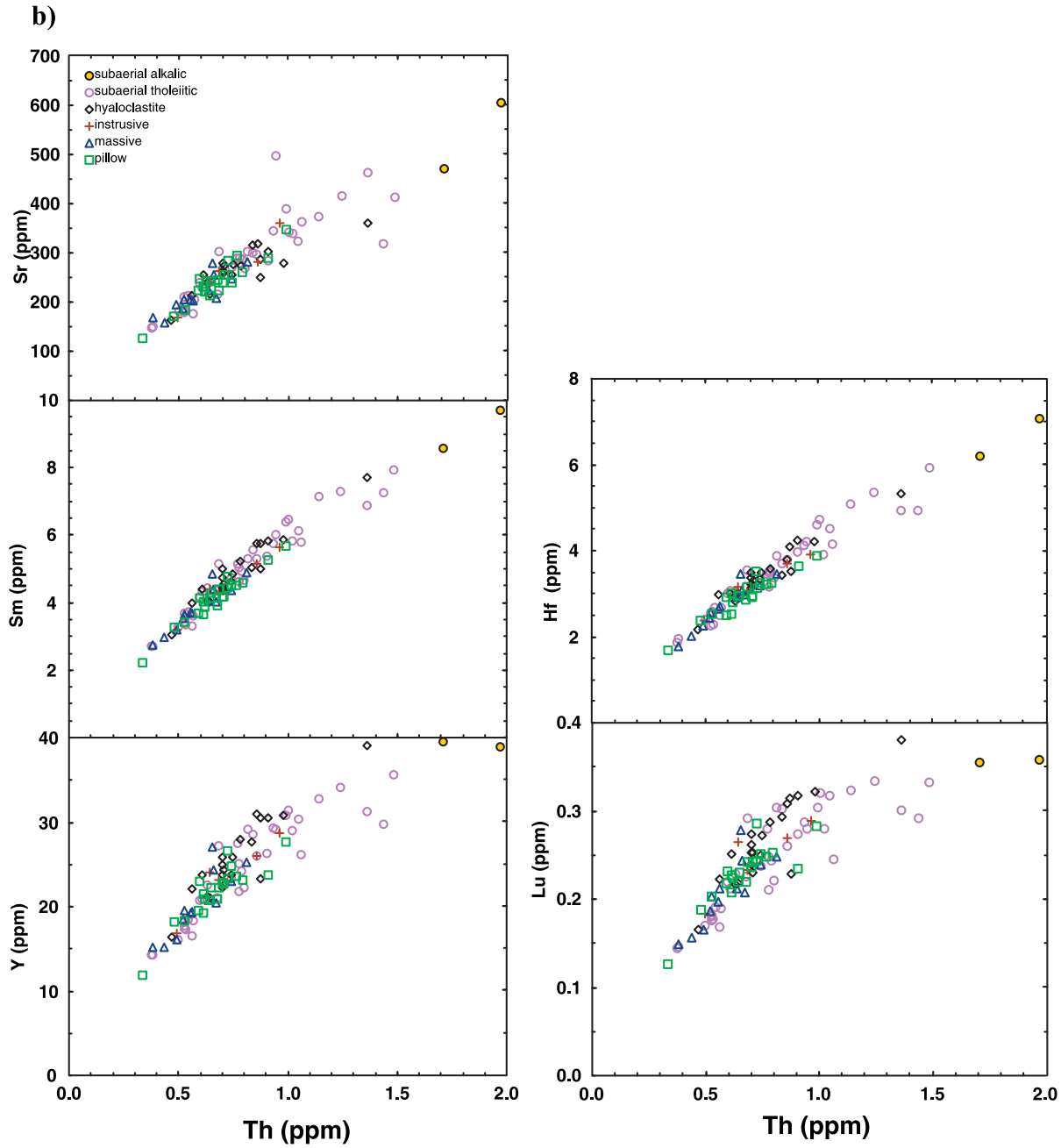

Figure 3. (continued)

Th are highly incompatible elements whose abundances were not affected by postmagmatic alteration. Abundance of Ba, Th and light REE are highly correlated, and in x-y plots the trends have near zero intercepts indicating that these elements were similarly incompatible (Figure 3a). The correlations are not as good for U, and especially Rb (Figure 3a); we infer that these poorer correlations reflect the effects of postmagmatic alteration [e.g., *Kennedy et al.*, 1991; *Cohen et al.*, 1996; *Yang et al.*, 1996, Huang, Vollinger, Frey and Rhodes, unpublished data, 2003]. Although Sr, Sm and Hf abundances versus Th abundance are also highly correlated, the trends clearly define convex upwards trends; such convexity is even more apparent for Y and heavy rare earth element abundance (Figure 3b). Non-linearity in abundance variation plots involving elements of differing incompatibility is characteristic of melts

derived by different extents of melting of a common source. This result arises from the mass balance equations

$$C^x_\ell/C^x_o = 1/[F + D_x(1-F)] \text{ and } (C^x/C^y)_\ell/(C^x/C^y)_o = [F + D_y(1-F)]/[F + D_x(1-F)]$$

(where x and y are generic incompatible elements; C^x_l and C^x_o are melt and source concentrations, respectively; F = melt fraction; D_x and D_y are bulk solid/melt partition coefficients). When Ds of incompatible elements are much less than the extent of melting (F), the abundance ratio $(C_x/C_y)_l$ is constant (i.e., trends with constant slope intersecting the origin in Figure 3a); therefore $(C_x/C_y)_l$ is independent of F and is equal to the source ratio. In contrast when Ds of incompatible elements are comparable to F, the abundance ratio $(C_x/C_y)_l$ varies with extent of melting; i.e., the slope changes in a x-y variation plot [e.g., *Hanson*, 1989, Figure 3]. The convexity in Figure 3b trends indicates that the bulk solid/melt partition coefficient for Th was smaller than that for Sr, Sm, Hf, Y and Lu.

Table 2. Comparison of Alkalic Basalt From HSDP Phase 1 and 2 Cores

	Phase 1		
	Analysis 1	Analysis 2	Phase 2
Reference Sample	R177-2.60		SR131-6.92
Flow Unit	58		48
Depth (m)	331.7		274.7
Age[a](Ka)	240 ± 14		234 ± 32
Isotopic Ratios[b]			
$^{87}Sr/^{86}Sr$	0.70356		0.703559
$^{176}Hf/^{197}Hf$	0.283129		0.283124
$^{206}Pb/^{204}Pb$	18.437		18.436
$^{207}Pb/^{204}Pb$	15.482		15.479
$^{208}Pb/^{204}Pb$	38.024		37.997
X-ray Fluorescence[c] (U. Mass.)			
SiO_2	43.68	43.60	43.75
TiO_2	3.96	3.95	3.99
Al_2O_3	14.39	14.38	14.40
Fe_2O_3	15.33	15.26	15.33
MnO	0.19	0.19	0.19
MgO	8.21	8.05	8.27
CaO	9.77	9.77	9.83
Na_2O	3.24	2.99	2.72(2.81)
K_2O	0.84	0.84	0.84
P_2O_5	0.47	0.48	0.49
Rb	15.0		13.8
Sr	628		613
Ba	253		242
V	267		271
Cr	116		134
Ni	151		137
Z	129		136
Y	34.8		34.1
R	287		283
Nb	28.0		27.3
Instrumental Neutron Activation[c] (MIT)			
Sc	25.5		25.8
Cr	127		129
La	23.7		23.6
Ce	59.3		59.6
Nd	36.5		39.1
Sm	9.00		9.30
Eu	3.13		3.10
Tb	1.31		1.40
Yb	2.40		2.41
Lu	0.33		0.33
Hf	6.58		6.61
Th	1.51		1.68

3. Discussion: HSDP Cores

3.1. Effects of Postmagmatic Alteration on Lava Compositions

[8] For subaerially erupted Hawaiian tholeiitic basalt, the abundance ratios K/Rb and K_2O/P_2O_5 are sensitive indicators of postmagmatic alteration because K and especially Rb are preferentially leached from the basalts leading to unusually low K_2O/P_2O_5 (<1) and high K/Rb (>1000) and Ba/Rb (>20) [e.g., *Feigenson et al.*, 1983; *Frey et al.*, 1991, 1994; *Yang et al.*, 1996]. For the HSDP samples the effects of such alteration are obvious in a plot of Ba/Rb versus K_2O/P_2O_5 where Ba/Rb, a ratio that is quite constant, 11.6 ± 0.2, in unaltered oceanic basalts [*Hofmann and White*, 1983], reaches values of >100 (Figure 4a). What is surprising about the

Notes to Table 2

[a] Argon isochron ages are for samples R177-6.0 and SR132-1.5 which are from the same units as the respective reference samples [*Sharp et al.*, 1998, submitted manuscript, 2002].

[b] Isotopic data from *Lassiter and Hauri* [1998], *Blichert-Toft and Albarede* [1999], *Abouchami et al.* [2000], Blichert-Toft et al. (submitted manuscript, 2002), Bryce and DePaolo (submitted manuscript, 2002).

[c] Oxides in wt.%, trace elements in ppm. Phase 1 abundances data from *Rhodes* [1996] and *Yang et al.* [1996]. The second column of major element data for R177-2.60 indicates result from a second (April, 2003) analysis; the agreement with the first analysis is excellent except for Na_2O which was the only significant difference between R177-2.60 and SR131-6.92. The new Na_2O value for R177-2.60 is in better agreement with the SR131-6.42 value. Phase 2 abundance data from Rhodes and Vollinger (submitted manuscript, 2002) and this paper. Na_2O value in parentheses was determined by INAA.

HSDP trend in Figure 4a is that the subaerial and submarine lavas define sub-parallel trends with the submarine lavas slightly offset to lower Ba/Rb at a given K_2O/P_2O_5. Submarine seawater alteration of MORB typically leads to increases in abundances of K and Rb [*Staudigel et al.*, 1995], but submarine HSDP samples show no evidence for addition of K and Rb. Alkali loss is especially characteristic of the second pillow zone (2234 to 2470 mbsl, see Figure 4b) which is composed of low density, vesicular pillow lava [*Moore*, 2001]. We infer that this pillow zone is a region of fresh water migration. Additional geochemical effects of postmagmatic alteration are discussed by *Chan and Frey* [2003] for lithium and M. J. Vollinger and J. M. Rhodes (Chemical alteration in basalts sampled by phase-2 of the Hawaii Scientific Drilling Project, manuscript submitted to *Geochemistry, Geophysics, Geosystems*, 2002) for major and trace elements.

3.2. Role of Crystal Fractionation

3.2.1. Plagioclase

[9] Only about 20% of the HSDP cores contains phenocrysts of plagioclase or clinopyroxene, and only a few of these lavas have >1% plagioclase or clinopyroxene phenocrysts [*Garcia et al.*, 1996; *DePaolo et al.*, 1999]. The role of plagioclase fractionation can be evaluated using Al_2O_3 abundance, $(Sr/Nd)_{PM}$ and relative abundance of Eu (subscript PM indicates normalized to primitive mantle). Samples from Phase 1 and 2 cores define an inverse correlation between Al_2O_3 and MgO (Figure 5a). The increased scatter at the low MgO end of the trend reflects the tendency of alkalic basalt to have higher Al_2O_3; e.g., samples SR 121, SR 131 and R177; tholeiitic sample SR 129 is also offset to high Al_2O_3 and CaO (Figures 5a and 5b). Since the Al_2O_3 content of plagioclase exceeds that of coexisting equilibrium melts, segregation of mineral assemblages including significant plagioclase result in decreasing Al_2O_3 abundance with increasing differentiation. Consequently, the inverse Al_2O_3 versus MgO trend shows that plagioclase fractionation was not an important process. Because Sr and Eu are relatively compatible in plagioclase the variation of $(Sr/Nd)_{PM}$ and (Eu/Eu*) with MgO content in an individual shield can also be used to evaluate the role of plagioclase fractionation. In general, HSDP Phase 2 samples have $(Sr/Nd)_{PM}$ close to unity, ranging from 0.8 to 1.2, and $(Sr/Nd)_{PM}$ does not vary systematically with MgO content (Figure 5c). Sample SR 129 has an anomalously high $(Sr/Nd)_{PM}$ >1.4 (Figure 5c). Also it is the sample with the largest enrichment in Eu (Eu/Eu* = 1.06, Figure 5d). Sample SR129 is from Unit 47 which contains up to 13% plagioclase phenocrysts [*DePaolo et al.*, 1999], and it is the only obvious plagioclase cumulate in the Phase 2 core.

[10] Sample SR125 has several anomalous geochemical characteristics. It has the lowest $(Sr/Nd)_{PM}$ (Figure 5c) and an unusually low Na_2O content (1.27%) which is confirmed by similar values determined by XRF and INAA (Rhodes and Vollinger, submitted manuscript, 2002) (Table 1 of this paper). This sample has a relatively high Loss on Ignition (3.43%), low K_2O/P_2O_5 (0.55) and high Ba/Rb (92) (Figure 4). It appears to have lost a plagioclase component during alteration; its CaO abundance, however, is not unusually low (Figure 5b), and Eu/Eu* is 0.98. In addition, it has an anomalously high Sc content (Figure 5e).

3.2.2. Clinopyroxene

[11] Clinopyroxene is also a rare phenocryst in HSDP lavas [*Garcia et al.*, 1996; *DePaolo et al.*, 1999]. The role of clinopyroxene fractionation can be evaluated using CaO and Sc abundances. The CaO versus MgO trend is inverse and like the Al_2O_3 versus MgO trend, there is more scatter at low MgO; in this case the scatter is caused by the relatively low CaO content of alkalic basalt (Figure 5b), perhaps indicating a role for clinopyroxene fractionation in generating alkalic basalt. Consistent with this inference some of the alkalic lavas, such as SR 131 and R177, have relatively low Sc and Cr contents (Figure 5e and Table 1). The only Phase 2 tholeiitic basalt which may have experienced clinopyroxene fractionation is SR 850 which has high abundances of incompatible elements (Figure 3a) and a low MgO content (6.44%); for this MgO content, it has relatively low Sc abundance (Figure 5e). However, no

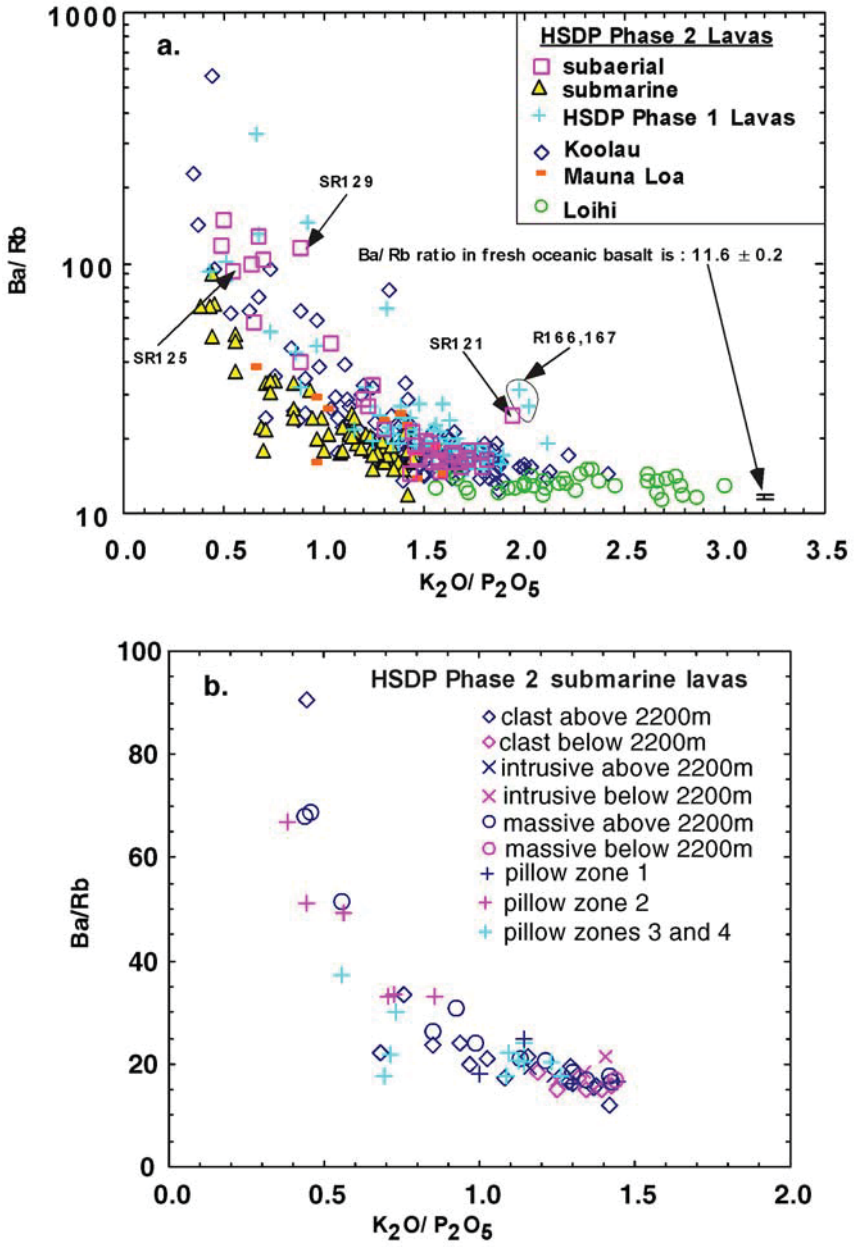

Figure 4. (a) Ba/Rb versus K_2O/P_2O_5 for basalt from the HSDP Phase 1 and 2 cores. K_2O and Rb abundances are decreased during subaerial alteration in the Hawaiian environment [e.g., *Yang et al.*, 1996]. Hence, the trend to low K_2O/P_2O_5 and high Ba/Rb reflects increasing amounts of postmagmatic alteration. Unaltered Hawaiian basalt has K_2O/P_2O_5 >1.5 and Ba/Rb close to that of average oceanic basalt (11.6 ± 0.2 [*Hofmann and White*, 1983]). It is surprising that submarine lavas from the HSDP Phase 2 core also define an inverse trend, which is offset to lower Ba/Rb. Data for HSDP Phase 1 from *Rhodes* [1996] and HSDP Phase 2 from Rhodes and Vollinger (submitted manuscript, 2002) and this paper. Shown for comparison are data for subaerial lavas from Koolau volcano [*Frey et al.*, 1994; *Jackson et al.*, 1999; *Haskins and Garcia*, unpublished data] which define the same trend as the subaerially erupted HSDP samples, and data for Mauna Loa [*Rhodes*, 1996] and for Loihi [*Garcia et al.*, 1993, 1995, 1998; *Norman and Garcia*, 1999]. (b) K_2O/P_2O_5 versus Ba/Rb for the various types of the HSDP Phase 2 submarine lavas. Lavas from above and below 2200 m are distinguished because below 2200 m the lavas are relatively undegassed, indicating eruption in a submarine environment [*Moore*, 2001]. An important result is that the trend to low K_2O/P_2O_5 and high Ba/Rb is in part defined by pillow lavas from >2200 m especially those from the vesicular pillow zone 2 that extends from 2234 to 2470 mbsl [*Moore*, 2001].

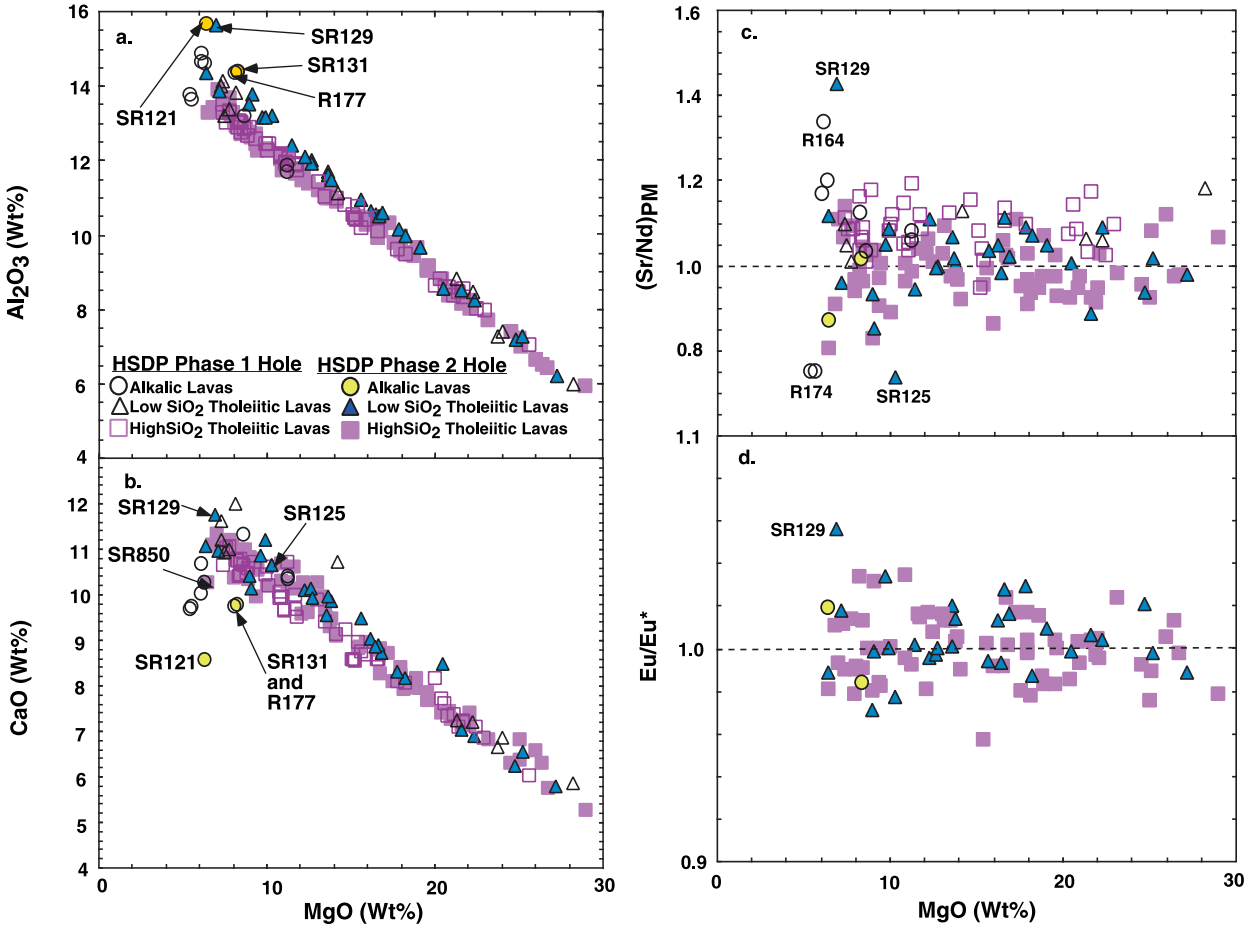

Figure 5. (a,b) Al_2O_3 and CaO versus MgO content (all in wt.%). Major oxide abundances are from Rhodes and Vollinger (submitted manuscript, 2002). The inverse trends dominantly reflect the effects of olivine fractionation and accumulation and perhaps magma mixing (Rhodes and Vollinger, submitted manuscript, 2002). In detail, however, the alkalic basalts at ~6 to 8% MgO scatter to high Al_2O_3 and low CaO; also a subgroup of the tholeiitic basalt from both holes which have relatively low SiO_2 (see Figure 6a) are slightly offset to higher Al_2O_3 at a given MgO content in the range of 6 to 14% MgO. (c,d) $(Sr/Nd)_{PM}$ and Eu/Eu* versus MgO content. Subscript PM indicates normalized to a primitive mantle ratio of 15.6 [*Sun and McDonough*, 1989]. Eu* is an estimate of Eu abundance based on extrapolation between Sm and Gd in a chondrite-normalized plot for REE and Eu is the measured abundance. These ratios are indicators of plagioclase accumulation. For $(Sr/Nd)_{PM}$ all samples are within 0.8 to 1.2 except for higher ratios for SR129 and R164 and lower values for R174 and SR125. The mean ratio in the Phase 1 core is >1 and larger than that in the Phase 2 core. Different analytical techniques were used (XRF and INAA for Phase 1, ICP-MS for Phase 2); hence the systematic differences probably reflect inter-laboratory bias. All Phase 2 samples have Eu/Eu* in the range 0.95 to 1.05, except for SR129 which has a ratio of 1.06. (e,f) Sc and Ni abundances (in ppm) versus MgO content (wt.%). The Sc trend is generally inverse, reflecting the incompatibility of Sc in olivine. The most obvious deviations are: the high Sc of SR125, a sample with many anomalous geochemical characteristics (see text); and the low Sc content (also Cr which is not plotted) of alkalic basalt R177 and SR131 which are from the same flow (Table 2). Sample SR 850 is the tholeiitic basalt with a low MgO content and high abundances of incompatible elements (Figure 3a); it is offset from the general trend to low CaO (panel b) and Sc, thereby indicating a role for clinopyroxene fractionation. Sc abundance determined by INAA (Table 1). The positive correlation between Ni and MgO abundance reflects olivine accumulation, but at <7% MgO, Ni contents become less variable, presumably because of combined plagioclase, clinopyroxene and olivine fractionation (Ni abundance data from Rhodes and Vollinger, submitted manuscript, 2002).

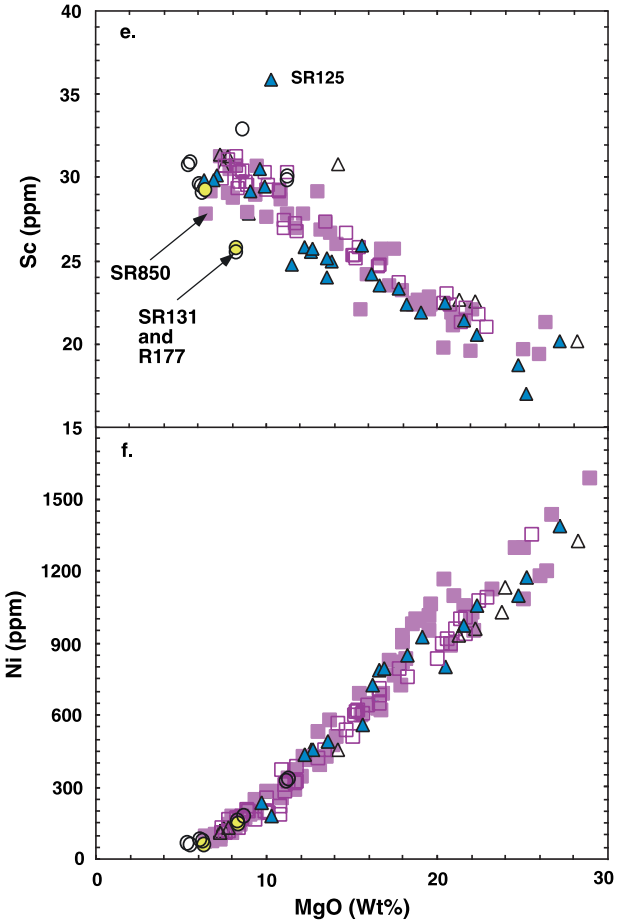

Figure 5. (continued)

clinopyroxene phenocrysts were observed in this sample [*DePaolo et al.*, 1999].

3.2.3. Olivine

[12] Olivine is the dominant phenocryst/xenocryst in most of the HSDP tholeiitic basalts and petrographic observation shows that in contrast to plagioclase and clinopyroxene fractionation, olivine accumulation and fractionation was an important process [e.g., *Baker et al.*, 1996; *Garcia et al.*, 1996; Rhodes and Vollinger, submitted manuscript, 2002]. A reflection of the role of olivine is the wide variation in MgO content (6% to 29%) and the positive correlation between MgO and Ni abundance (Figure 5f). In order to adjust for the effects of olivine fractionation and accumulation for each of the Phase 2 lavas, we added or subtracted olivine in 1% increments with $K_D^{Fe/Mg} = 0.3$ until the calculated composition was in equilibrium with Fo_{90} olivine, typical of the most Mg-rich olivine phenocrysts in the core, or Fo_{85} which is closer to the average olivine composition [*Baker et al.*, 1996; *Garcia et al.*, 1996]. This adjustment greatly reduces the MgO variation (~10 to 13% for Fo_{85} and ~16.6 to 19.6% for Fo_{90}), and decreases the abundance range of incompatible elements (Figure 2a). In summary, olivine addition and fractionation was a dominant process controlling the compositions of HSDP lavas (see also Rhodes and Vollinger, submitted manuscript, 2002). Although this process can explain much of the variation in abundance of incompatible elements (Figures 2 and 3), it cannot explain the convexity of trends in Figure 3b.

3.3. Geochemical Groups in HSDP Cores

3.3.1. Postshield Group

[13] As with Al_2O_3 and CaO versus MgO abundance (Figures 5a and 5b), the abundance of SiO_2 and TiO_2 are scattered at low MgO content because the eleven samples of alkalic basalt (nine in Phase 1 core and two in Phase 2 core) in the upper part of the cores have relatively low SiO_2 and high TiO_2 content (Figures 6a and 6b) and relatively high total iron contents [*Rhodes*, 1996; Rhodes and Vollinger, submitted manuscript, 2002]. The upper 152 m of the Mauna Kea section in the Phase 2 core (samples SR121 through SR175) includes intercalated alkalic and tholeiitic basalt which define a trend to relatively low SiO_2 content (Figures 7c and 7f). In the range of 6 to 10% MgO, at a given MgO content these low SiO_2 lavas within the upper 152 m have the highest abundance of Nb and other incompatible elements (Figure 3a), Al_2O_3 (Figure 5a) and TiO_2 (Figure 6b). Although there is considerable scatter in downhole trends for incompatible element abundance ratios, such as Nb/Zr and La/Yb, these ratios are relatively high in the alkalic samples SR 121 and SR 131 near the top of the Mauna Kea section (Figures 7a and 7b). Moreover, within the uppermost Mauna Kea lavas, there is a trend to relatively high Nb/Zr and La/Yb with decreasing depth and age (Figures 7a, 7b, 7d, and 7e).

[14] The age range of samples SR121 to SR175, ~200 ka to 330 ka (Figure 7f), overlaps with the oldest of the Hamakua Volcanics, ~70 ka to 250 ka,

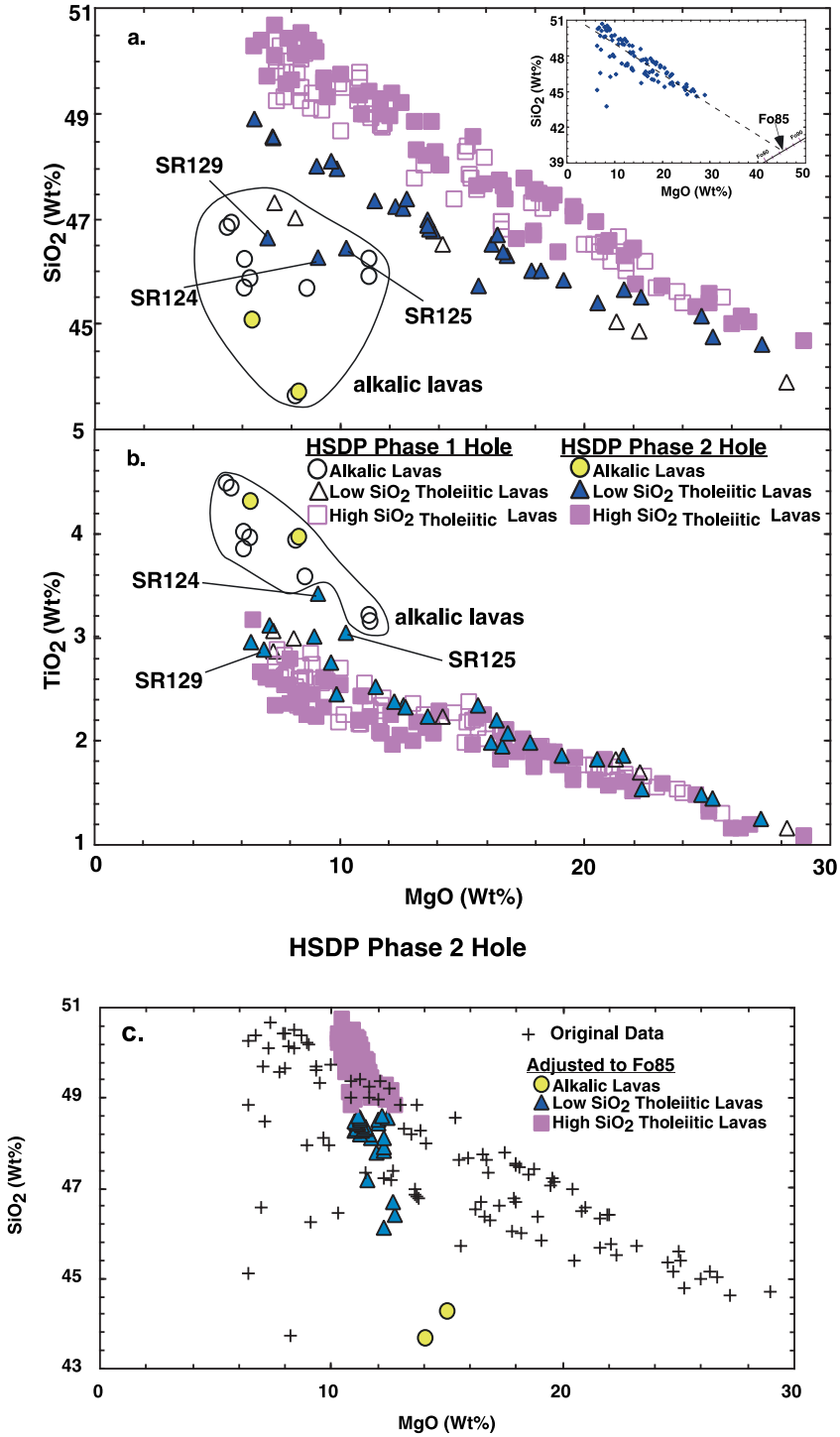

Figure 6. (a,b) SiO_2 and TiO_2 versus MgO content (all in wt.%). The alkalic lavas including the three labeled tholeiitic lavas from the upper part of the Mauna Kea section, are offset to relatively low SiO_2 and high TiO_2 contents. Also there is a subgroup of tholeiitic lavas with relatively low SiO_2 at a given MgO content. These two subsets of tholeiitic lavas are labeled as low and high SiO_2 lavas. Inset shows that the main trend of data for SiO_2-MgO intersects the trajectory of olivine compositions at $\sim Fo_{85}$. (c) SiO_2 versus MgO content (wt.%) showing the abundance range after adjusting each sample to be in equilibrium with Fo_{85}. This adjustment reduces the range of MgO abundance, but a significant range in SiO_2 content persists.

which form the basaltic postshield stage that is exposed on the lower subaerial flanks of Mauna Kea volcano [*Frey et al.*, 1990, 1991; *Wolfe et al.*, 1997]. The Hamakua Volcanics also include intercalated tholeiitic and alkalic basalt. *Yang et al.* [1996, Figure 9] showed that the trend to high La/Yb at the top of the Phase 1 core is continuous with that defined by the Hamakua Volcanics. Therefore, we refer to the intercalated alkalic and tholeiitic basalt in the upper parts of the Phase 1 and 2 cores as the Postshield Group. The gradual increase of La/Yb and Nb/Zr with decreasing age shows that the transition from shield to postshield stage was gradual and prolonged over a span of

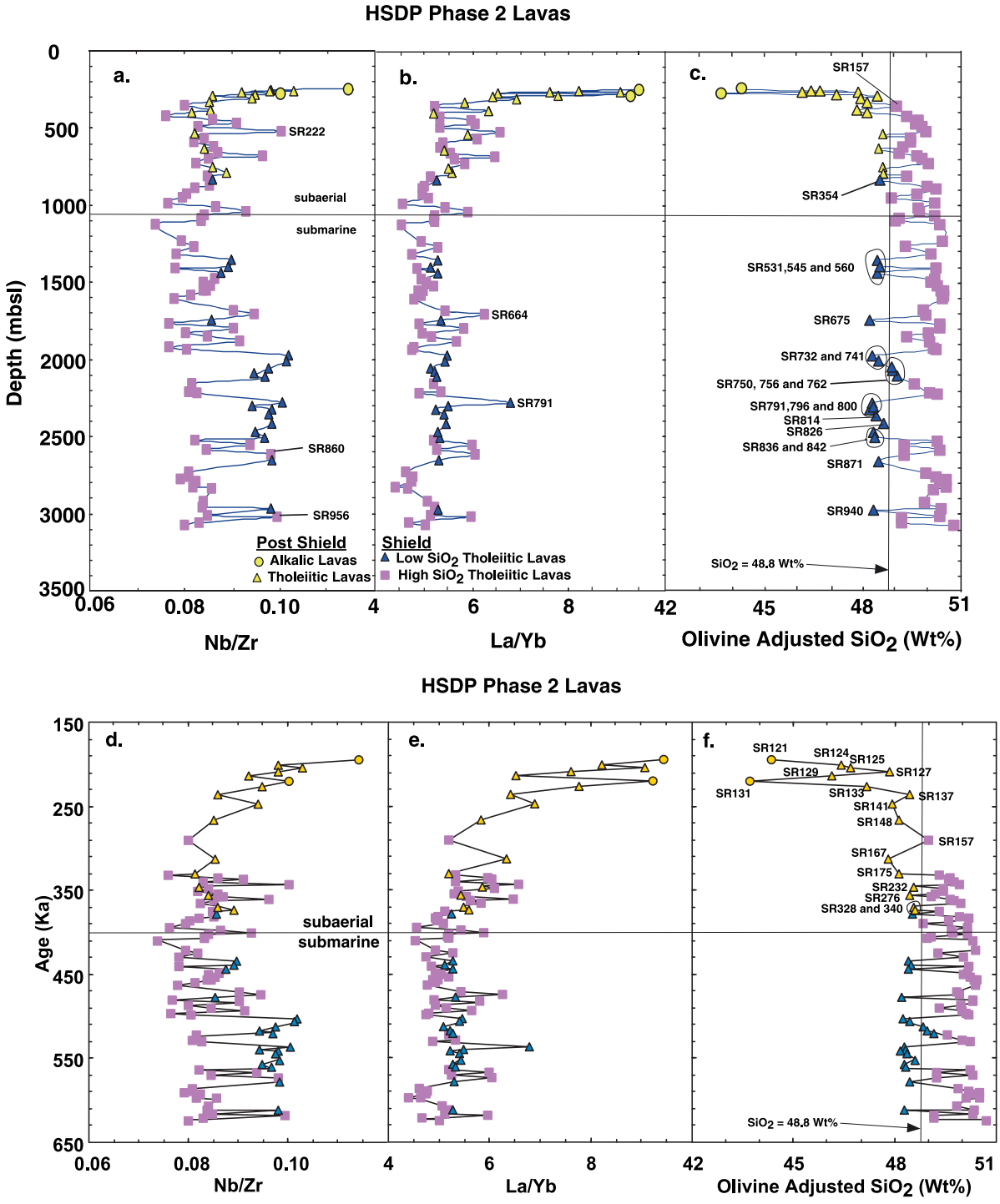

~130 ka (Figures 7d and 7e). Also, during the shield to postshield transition there were systematic changes in radiogenic isotopic ratios. For example, beginning at ~830 m $^3He/^4He$ decreases upward in the core (Figure 8a). The Postshield Group also has relatively low $^{206}Pb/^{204}Pb$, $^{208}Pb/^{204}Pb$ and ε_{Hf}, but relatively high ε_{Nd} (Figures 8b, 8c, 8d, and 8e). Based on their relatively low SiO_2 (Figures 7c and 7f), $^3He/^4He$ (Figure 8a) and $^{208}Pb/^{204}Pb$ at a given $^{206}Pb/^{204}Pb$ (Figure 8f), we include samples of SR232, SR276, SR328 and SR340 in this Postshield Group, thereby increasing the initiation of postshield volcanism to ~370 ka (Figure 7f).

3.3.2. Low SiO_2 Shield Group

[15] Lavas with relatively low SiO_2 content (Figures 6a and 6c) are not restricted to the Postshield Group. In the Phase 2 core some of the deeper and older (>834 mbsl and >380 ka) lavas have relatively low SiO_2 content (Figures 7c and 7f). We identify these as the Low SiO_2 Shield Group (individual samples are labeled in Figure 7c). This group is characterized by relatively high $^3He/^4He$ and high $^{208}Pb/^{204}Pb$ at a given $^{206}Pb/^{204}Pb$, Figures 8a and 8f). Based on these isotopic parameters, the youngest lava in the Low SiO_2 Shield Group is subaerial sample SR354, and samples SR750, SR756 and SR762 also belong to this group (Figures 8a and 8f), despite their adjusted SiO_2 contents of >48.8% (Figure 7c); that is we conclude that the arbitrary SiO_2 discriminant does not perfectly identify this group. In part this difficulty arises from SiO_2 mobility during postmagmatic alteration (Vollinger and Rhodes, submitted manuscript, 2002). In addition, as we emphasize in later discussion, there is within group variation in geochemical characteristics, e.g., La/Yb and Zr/Nb; that is some samples are transitional between the groups. Nevertheless $^3He/^4He$ and delta $^{208}Pb/^{204}Pb$ clearly distinguish the Low SiO_2 Shield Group (Figure 8).

3.3.3. High SiO_2 Shield Group

[16] Most of the lavas have adjusted SiO_2 contents >48.8% (Figure 7c and 7f), and they define the main inverse trends in MgO variation plots (Figures 5 and 6). These samples form the High SiO_2 Shield Group.

3.4. Comparison of Geochemical Groups Defined by Huang and Frey (this paper) With Those Defined by Rhodes and Vollinger (submitted manuscript, 2002)

[17] Rhodes and Vollinger (submitted manuscript, 2002) used adjusted SiO_2 content and Zr/Nb as principle criteria for defining lava types in the Phase 2 core whereas we use adjusted SiO_2 content, incompatible element abundance ratios, $^3He/^4He$ and Pb isotopic ratios to define geochemical groups. Consequently, the lava types defined by Rhodes and Vollinger (submitted manuscript, 2002) are generally similar to our groups, but there are some important differences.

3.4.1. Postshield

[18] Rhodes and Vollinger (submitted manuscript, 2002) include only samples SR121 (246.2 mbsl)

Figure 7. (opposite) (a,b,c) Nb/Zr, La/Yb, and SiO_2 contents (adjusted to be in equilibrium with olivine of Fo_{85}) versus depth in the HSDP Phase 2 core in meters below sea level (mbsl). Significant results are the high Nb/Zr and La/Yb in 12 of the uppermost 13 lavas. These lavas also have relatively low SiO_2 contents; in each plot the most extreme values are for alkali basalt samples SR121 and SR131, but 10 of the uppermost 11 tholeiitic lavas also have relatively low SiO_2 content. These samples are defined as the Postshield Group. Samples SR232, SR276, SR328 and SR340 are also included in this group (see text). Underlying samples with relatively low SiO_2, labeled samples SR354 through SR940 in Figure 7c, are defined as the Low SiO_2 Tholeiitic Shield Group. The 48.8% SiO_2 dividing line is arbitrary, and samples SR750, 756 and 762 with >48.8% SiO_2 are included in this group (see text). In Figure 7a the 3 labeled high Nb/Zr samples are Type 4 of Rhodes and Vollinger (submitted manuscript, 2002). In Figure 7b two samples with anomalously high La/Yb are labeled; their relatively high ratios are confirmed by the data of Feigenson et al. (submitted manuscript, 2002). (d,e,f) La/Yb, Nb/Zr and SiO_2 contents (adjusted to be in equilibrium with olivine of Fo_{85}) versus age in the HSDP Phase 2 core. Inferred ages are from Sharp et al. (submitted manuscript, 2002). These panels show the prolonged transition from the shield groups to the postshield group. The age span from SR121 to SR340 is ~180 Ka.

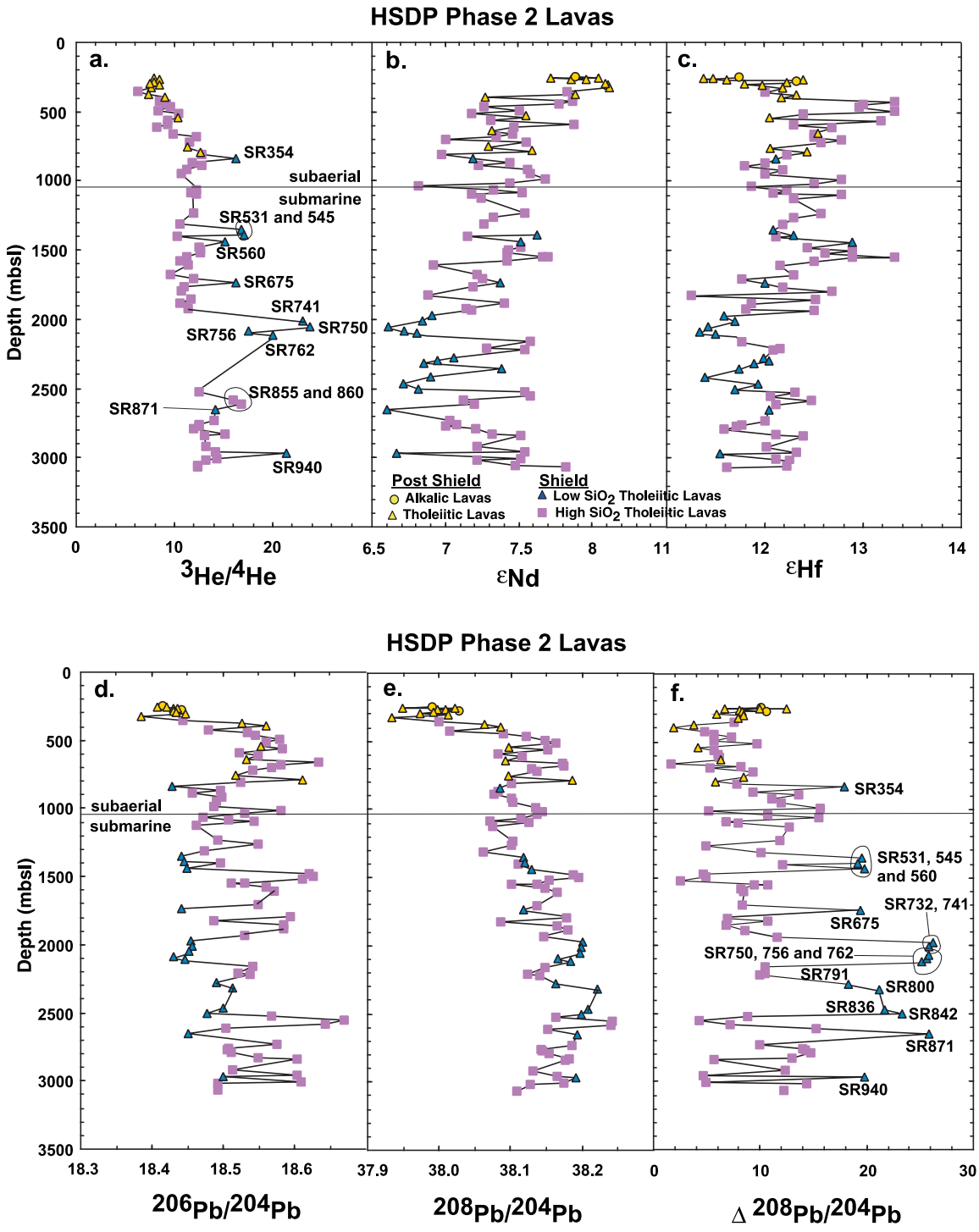

Figure 8. (a-f) Depth profiles for isotopic ratios: $^{3}He/^{4}He$; ε_{Nd}; ε_{Hf}; $^{206}Pb/^{204}Pb$, $^{208}Pb/^{204}Pb$ and delta $^{208}Pb/^{204}Pb$ (delta $^{208}Pb/^{204}Pb = [(^{208}Pb/^{204}Pb) - (^{208}Pb/^{204}Pb)_{NHRL}] \times 100$ where NHRL is northern hemisphere reference line [see *Hart*, 1984]. ε_{Nd} and ε_{Hf} are related to $^{143}Nd/^{144}Nd$ and $^{176}Hf/^{177}Hf$, respectively (see Bryce and DePaolo, submitted manuscript, 2002; Blichert-Toft et al., submitted manuscript, 2002). The Postshield Group and intercalated subaerial High SiO_2 Tholeiitic lavas have relatively low $^{3}He/^{4}He$, high ε_{Nd}, low ε_{Hf} and low $^{206}Pb/^{204}Pb$, $^{208}Pb/^{204}Pb$ and delta $^{208}Pb/^{204}Pb$. In contrast, the labeled lavas forming the Low SiO_2 Shield Group are distinguished by relatively high $^{3}He/^{4}He$ (SR871 is anomalously low) and relatively high delta $^{208}Pb/^{204}Pb$. Data sources are Kurz et al. (submitted manuscript, 2002) for He; Bryce and DePaolo (submitted manuscript, 2002) for Sr and Nd, Blichert-Toft et al. (submitted manuscript, 2002) for Hf and Pb.

through SR152 (337 mbsl) in this type. We extend this grouping to include samples SR167, SR175, SR232, SR276, SR328 and SR340 (794 mbsl) that also have relatively low SiO_2 (Figure 7f).

3.4.2. Type 1 of Rhodes and Vollinger (submitted manuscript, 2002)

[19] These are the dominant type of tholeiitic basalt in the core (61% of the Mauna Kea lavas analyzed by Rhodes and Vollinger (submitted manuscript, 2002)). They are present from 337 to 3098 mbsl and are equivalent to the High SiO_2 Shield Group in Figures 7c and 7f.

3.4.3. Type 2 of Rhodes and Vollinger (submitted manuscript, 2002)

[20] This type includes low SiO_2 lavas restricted to the upper part of the Mauna Kea section (above 1739 mbsl); these lavas are most abundant between 337 and 850 mbsl. This type includes tholeiitic lavas that resemble tholeiitic basalt occurring within the postshield group. Rhodes and Vollinger (submitted manuscript, 2002) include low SiO_2 subaerial lavas SR276, SR328, SR340 and SR354, as well as the low SiO_2 submarine lavas SR531, SR545, SR560 and SR675 in this type (Figure 7c). Because of their relatively high $^3He/^4He$ and delta $^{208}Pb/^{204}Pb$ (Figures 8a and 8f) we include samples SR354, SR531, SR545, SR560 and SR675 in our Low SiO_2 Shield Group. These samples, however lack the high Nb/Zr that distinguishes older lavas in this group (Figures 7a and 7d). We agree that samples SR276, SR328 and SR340 are similar to the Postshield group and we include them in this group (Figures 7 and 8).

3.4.4. Type 3 of Rhodes and Vollinger (submitted manuscript, 2002)

[21] These are low SiO_2 lavas confined to the submarine portion of the core. They are equivalent to our Low SiO_2 Shield Group. They are a distinctive group because low SiO_2 is coupled with relatively high Nb/Zr, $^3He/^4He$ and delta $^{208}Pb/^{204}Pb$ (Figures 7a, 7d, 8a, and 8f). As noted by Rhodes and Vollinger (submitted manuscript, 2002) these are also characteristics of Loihi lavas. An important difference in our grouping is that sample SR354 is a Type 2 sample in the Rhodes and Vollinger classification because it has "normal" Nb/Zr, low SiO_2 and is in the subaerial part of the core. However, it has relatively low SiO_2, high $^3He/^4He$ and delta $^{208}Pb/^{204}Pb$; these are characteristics of of our Low SiO_2 Shield Group (Figures 7c, 7f, 8a, and 8f). This sample is important because it occurs high in the core within the subaerial section (834 mbsl with an inferred age of 380 ka). It is the uppermost sample of our Low SiO_2 Shield Group.

3.4.5. Type 4 of Rhodes and Vollinger (submitted manuscript, 2002)

[22] This type includes only 4 samples (two are from unit 92) and is defined by relatively high Nb/Zr but they do not have relatively low SiO_2 contents. We analyzed three of these samples (SR222, SR860 and SR956) and also find that they have relatively high Nb/Zr (Figure 7a). However, unlike Group 3 lavas, they do not have relatively high $^3He/^4He$ and delta $^{208}Pb/^{204}Pb$ (Figures 8a and 8f); therefore, we do not recognize them as a distinct group.

3.5. Petrogenesis of Geochemical Groups

3.5.1. Postshield Group

[23] The abundance ratios La/Sm, La/Yb, Sm/Yb and Nb/Zr are positively correlated with incompatible element content in the Postshield Group (e.g., Th in Figure 9), and the highest La/Yb and Nb/Zr ratios are in samples from the upper part of the core (Figures 7a, 7b, 7d, and 7e). Although radiogenic isotope ratios vary systematically with depth in this group (Figure 8), a plausible inference is that changes in proportions of source components were accompanied by variations in extent of melting with the alkalic lavas representing the lowest degree of melting [*Yang et al.*, 1996]. To test this hypothesis we did forward modeling for partial melting of spinel- and garnet-peridotite (see Figure 10 and Appendix B). The relatively large variations of La/Yb, Nb/Zr and Sm/Yb within the Postshield Group (Figures 10a, 10b, and 10c) are consistent with variable extents of batch melting of garnet

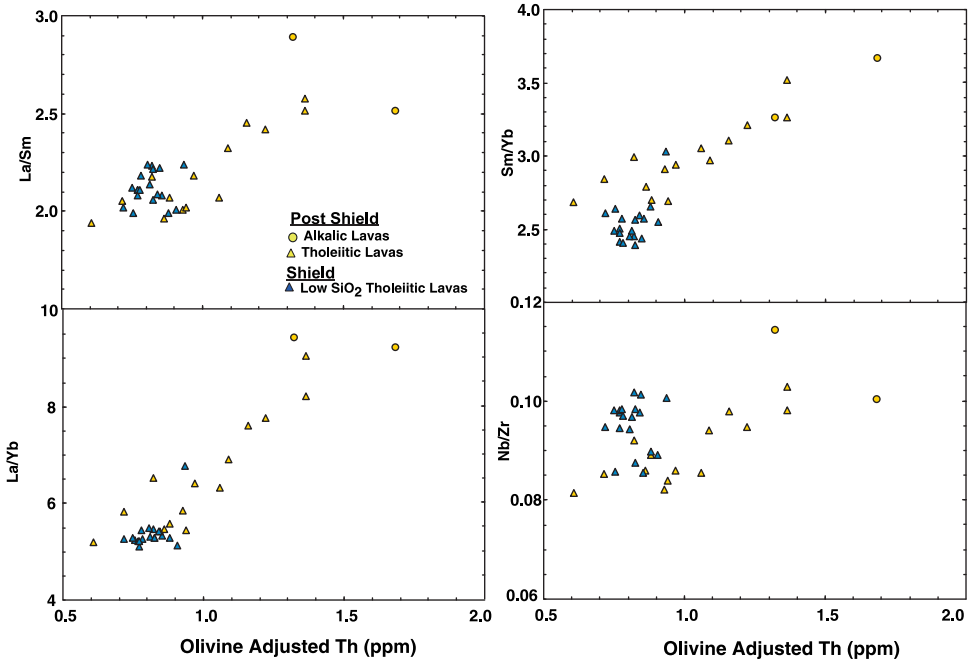

Figure 9. La/Sm, La/Yb and Nb/Zr versus Th content (adjusted so that each sample has a Mg/Fe ratio in equilibrium with olivine of Fo_{85}) for two groups of Phase 2 Mauna Kea lavas.

peridotite with La/Yb, Nb/Zr and Sm/Yb ratios slightly greater than estimates for primitive mantle (Table A4 of Appendix B). It is surprising that the range in La/Yb and Nb/Zr in the Postshield Group is similar to that for historical, ~200 yr, Kilauea lavas (Figure 10e). These variations in Kilauea shield lavas have been explained by a factor of two change in extent of melting of garnet peridotite [*Pietruszka and Garcia*, 1999].

[24] Segregation of the primary magmas for the Postshield Group within the stability field of

Figure 10. (opposite) (a,b,c,d) La/Yb and Sm/Yb versus Nb/Zr, and La/Yb versus Sm/Yb and Ti/Zr in HSDP Phase 2 samples. Symbols as defined in Figure 8. In Figures 10a, 10b, and 10c there are positive correlations with the highest La/Yb and Sm/Yb ratios in the uppermost samples in the Mauna Kea part of the core (also see Figures 7b and 7e). The difference between the two groups of shield lavas is significant in the La/Yb and Sm/Yb versus Nb/Zr panels where the Low-SiO_2 Group shows relatively little variation in La/Yb and Sm/Yb (sample SR 791 is an exception) and an inverse trend for Sm/Yb versus Nb/Zr. This group also ranges to the highest Ti/Zr found in the Mauna Kea portion of the core. The relatively high La/Yb for SR 791 is confirmed by the data of Feigenson et al. (submitted manuscript, 2002). SR791 at a depth of ~2280 m is from Unit 288 which is a thick sequence of pillows [*DePaolo et al.*, 1999]. ICP-MS data are used in Figures 10a, 10b, and 10c; in Figure 10d La and Yb are ICP-MS data, Ti and Zr are XRF data from Rhodes and Vollinger (submitted manuscript, 2002). In each panel calculated melting trajectories are shown for batch partial melting (1% increments with total extents of melting indicated at both ends of the trajectories) of spinel peridotite, and garnet peridotite. Details of the models, such as source abundances, mineral modes, melting reactions, and mineral/melt partition coefficients, are in appendix II. (e,f,g) Panels are equivalent to Figures 10a and 10d, but their objective is to compare Phase 2 Mauna Kea lavas with shield lavas from Kilauea, Mauna Loa and Loihi. Figure 10e shows that Phase 2 Mauna Kea Shield lavas are intermediate between historic Kilauea lavas [*Pietruszka and Garcia*, 1999] and historic Mauna Loa lavas [*Rhodes and Hart*, 1995]. Most notable is that the range of La/Yb and Nb/Zr during the last 200 years of Kilauea volcanism (dashed field) exceeds that of the >300,000 years of Mauna Kea volcanism recorded in the Phase 2 core. Figures 10f and 10g show data for Loihi seamount. At high ratios, the trend labeled "Loihi lavas" reflects the higher ratios of alkalic lavas created by the lower degrees of melting [*Frey and Clague*, 1983; *Garcia et al.*, 1993]. Most important is the Loihi Glasses field (outlined in blue and from *Garcia et al.* [1998]) which shows that recent tholeiitic glasses from Loihi seamount have relatively high Nb/Zr and Ti/Zr overlapping with the Low SiO_2 Shield Group of Mauna Kea. The field labeled Loihi Picrites (outlined in red and from *Norman and Garcia* [1999]) also has high Nb/Zr but in contrast to the glasses, these picrites do not have La/Yb and Ti/Zr similar to the Low SiO_2 Group of Mauna Kea lavas.

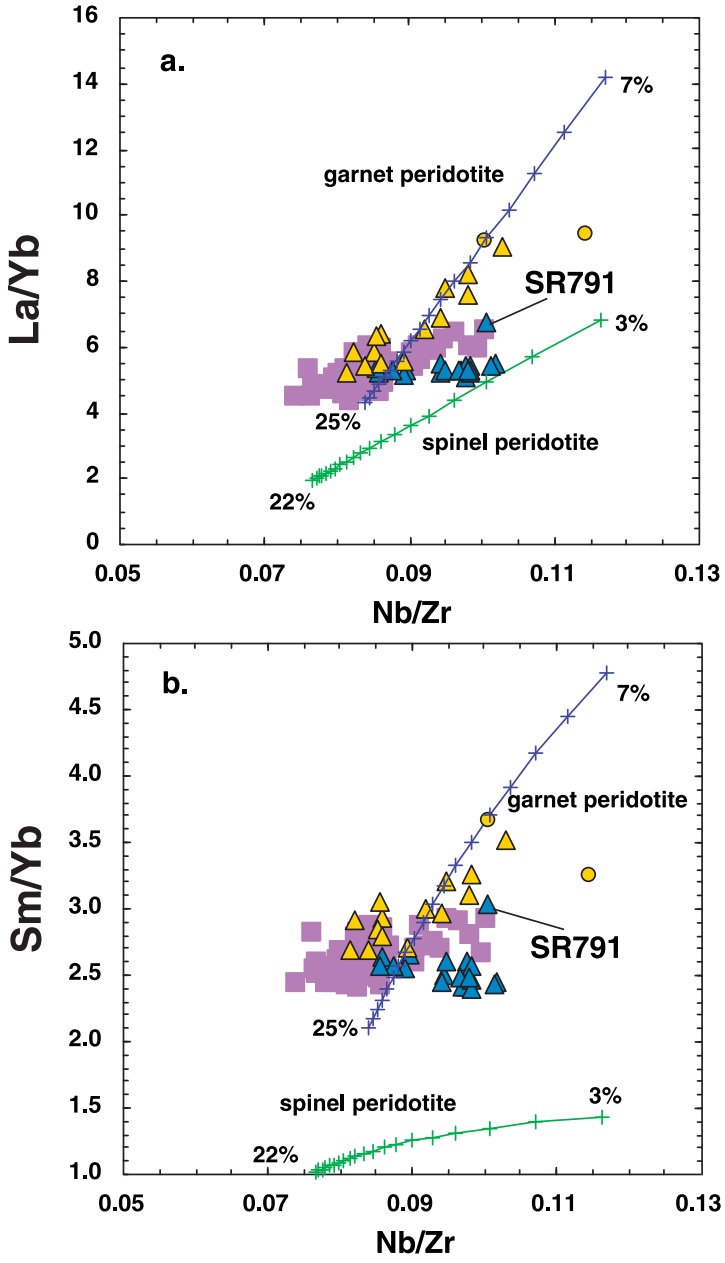

garnet is consistent with the inverse modeling of rare earth element abundances by M. D. Feigenson et al. (Partial melting and fractional crystallization of Mauna Kea lavas: Evidence from rare earth element concentrations of HSDP basalts, manuscript submitted to *Geochemistry Geophysics Geosystems*, 2003) who inferred that alkalic lavas in the upper part of the core formed by low degrees of melting of a garnet-bearing source. In addition, we suggest that the Ti/Zr ratio is useful for identifying a role for residual garnet because $D^{Ti/Zr}_{cpx/melt} > 1$ whereas $D^{Ti/Zr}_{gt/melt} < 1$, especially for Ca-rich garnet (Table A4). The Postshield Group trend of varying La/Yb at nearly constant Ti/Zr is clearly most consistent with partial melting of garnet peridotite (Figure 10d). Melt segregation of the postshield lavas at relatively high pressure is also consistent with their relatively low SiO_2 content (Figure 7f) and high FeO content (Rhodes and Vollinger, submitted manuscript, 2002, Figure 6). Hence the petrogenetic inferences for the Postshield Group are consistent with the "overall trend of increasing

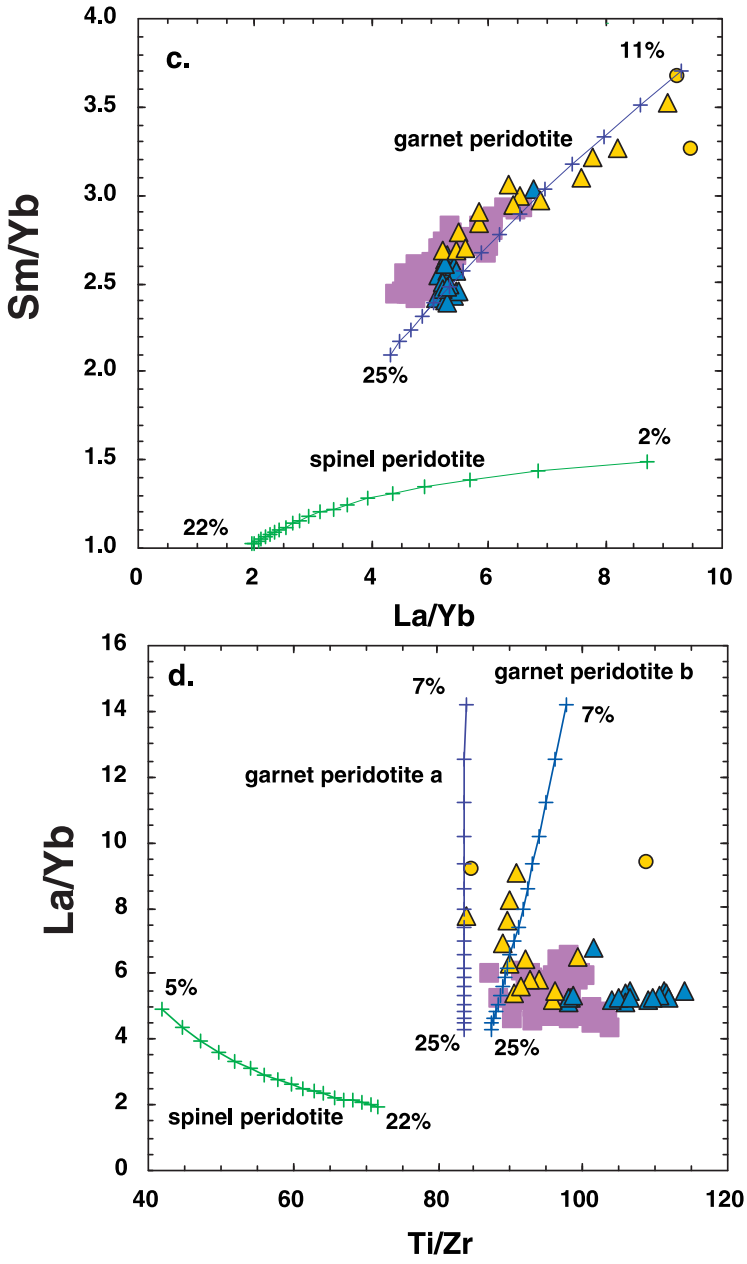

Figure 10. (continued)

pressure of melt segregation and decreasing extent of melting with decreasing eruption age" inferred by *Yang et al.* [1996] for the HSDP 1 core.

[25] In addition to variable extents of melting, Mauna Kea postshield lavas experienced more extensive crustal processing than shield lavas; for example, samples showing the effects of plagioclase or clinopyroxene fractionation are dominantly confined to subaerially erupted lavas (Figure 5). Moreover, samples with relatively low (~7%) MgO content are also abundant in the upper part of the Phase 2 core (Rhodes and Vollinger, submitted manuscript, 2002, Figure 5). The relatively low MgO content and a role for fractionation of plagioclase and clinopyroxene in the upper part of the core are consistent with longer residence times in crustal magma reservoirs as the magma supply from the mantle decreased during the transition from shield-stage to postshield-stage volcanism

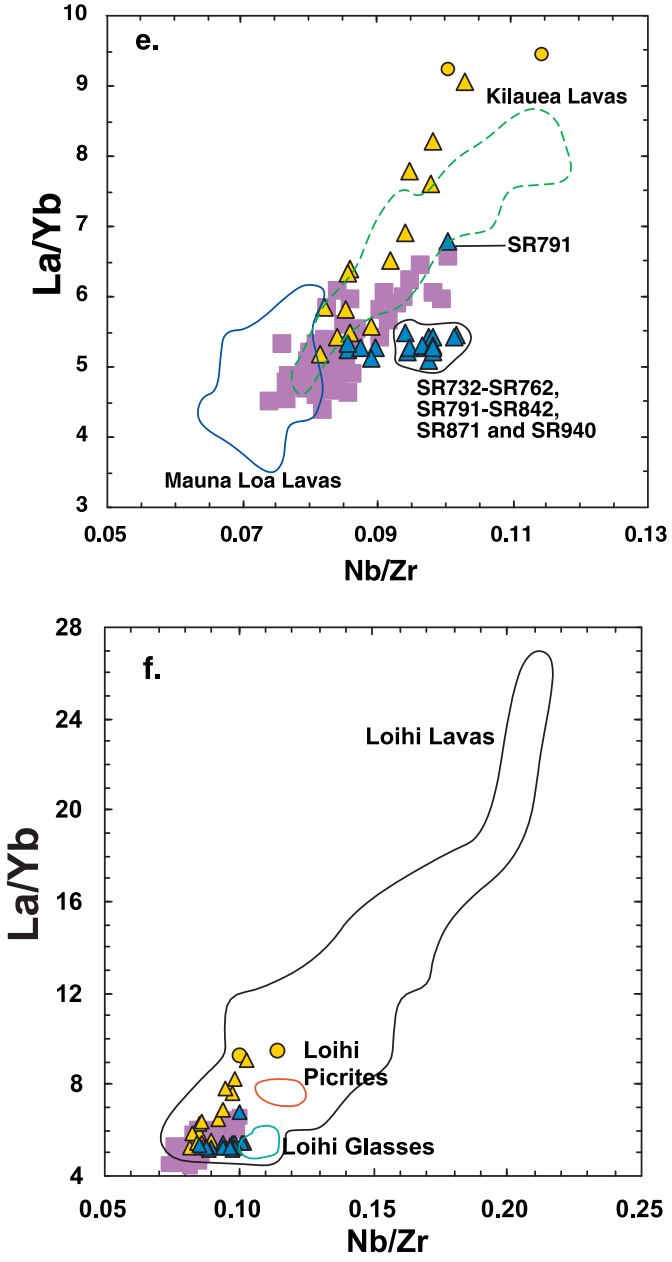

Figure 10. (continued)

[e.g., *Frey et al.*, 1990, 1991; *DePaolo and Stolper*, 1996].

3.5.2. Shield Groups

[26] The trends in Figure 10 for the High SiO_2 Shield Group are not as clearly defined as those for the Postshield Group, but they may also reflect variations in extent of melting. However, variations in radiogenic isotopic ratios within the core and even within the defined lava groups (Figure 11) shows that the petrogenesis of each group is more complex than variable extents of melting of a geochemically homogeneous source. As an example, the inverse Sm/Yb-Nb/Zr trend (Figure 10b) and relatively constant La/Yb but variable Ti/Zr of the Low SiO_2 Shield Group (Figure 10d) are inconsistent with variable extents of melting of a common peridotite source. Rhodes and Vollinger (submitted manuscript, 2002) noted that each of their major lava types ranges widely in

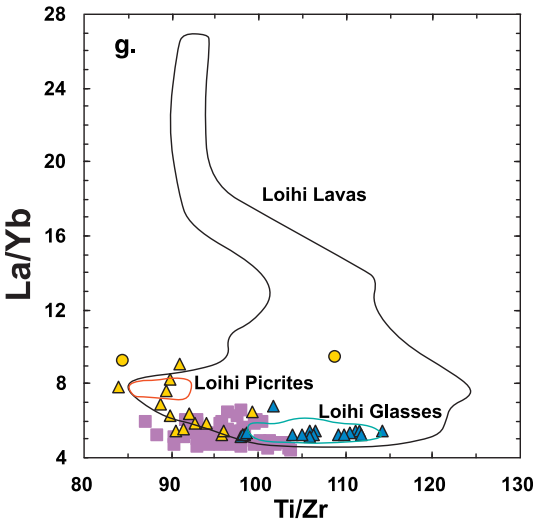

Figure 10. (continued)

MgO content. They argued that the near linear trends in MgO variation plots (e.g., Figures 5a, 5b, 6a, and 6b) reflect magma mixing in addition to olivine accumulation and fractionation. Although this complexity does not mask the compositional groups that we identify, the recognition of magma mixing as a significant process is important in explaining geochemical variations within these groups because the mixing end-members may be derived from geochemically distinct sources.

[27] An important observation is that the high Ti/Zr and Nb/Zr portion of the trends defined by the Low SiO_2 Shield Group is defined by the low SiO_2 lavas erupted in two distinct intervals (Figure 10e), the 5 samples from SR732 to SR762 (depth range of 1974 to 2124 mbsl and inferred age range of 503 ka to 520 ka) and the 7 samples from SR791 to SR842 (depth range of 2280 to 2504 mbsl and inferred age range of 537 ka to 561 ka). Also, a lower pillow basalt SR871 and intrusive sample SR940 are included in this subgroup. In addition to high Ti/Zr and Nb/Zr and relatively low SiO_2 contents these samples have relatively high $^3He/^4He$ (Figure 8a), and they define the low $^{206}Pb/^{204}Pb$ end of the Kea high 8 Pb array of Figure 2 in J. Eisele et al. (The long-term Pb isotope evolution of Mauna Kea lavas from the HSDP-2 drill core, manuscript submitted to *Geochemistry Geophysics Geosys-*

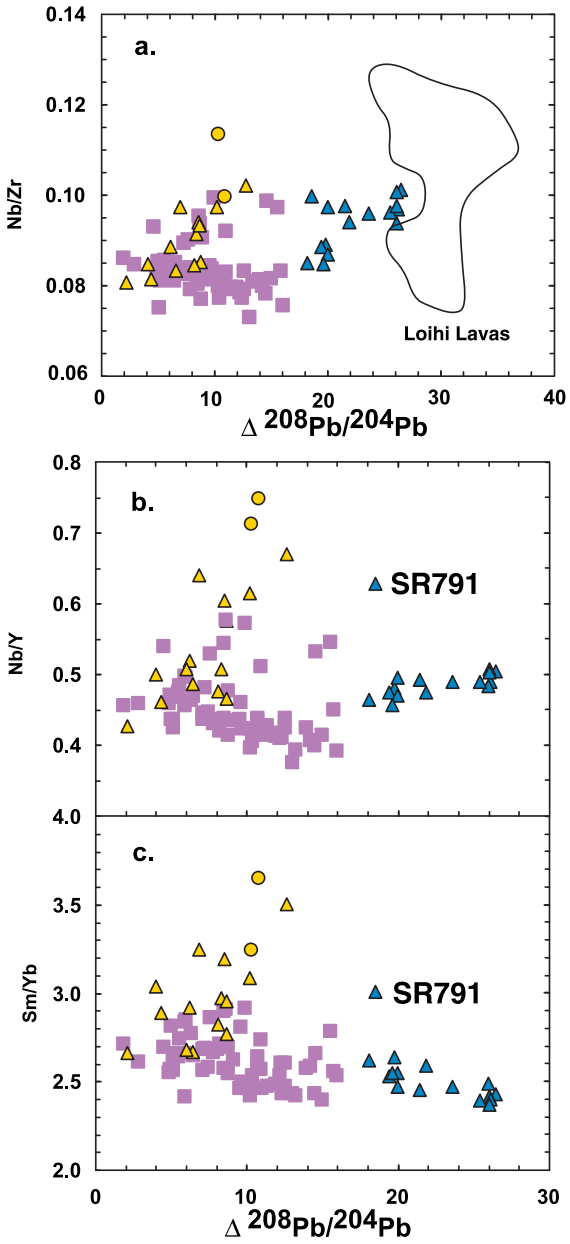

Figure 11. Delta $^{208}Pb/^{204}Pb$ (see Figure 8 for definition) versus the incompatible element abundance ratios, Nb/Zr, Nb/Y and Sm/Yb. Within each group of Mauna Kea lavas (symbols defined in Figure 8) these abundance ratios correlate with delta $^{208}Pb/^{204}Pb$. Sample SR791 is an anomalous member of the Low SiO_2 Shield Group. It is also distinguished by having the lowest Ba/Th ratio (Figure 15). The Low SiO_2 Shield Group ranges to high delta $^{208}Pb/^{204}Pb$ and it overlaps with the field for lavas from Loihi seamount (Figure 11a). In these panels the array of Mauna Kea data requires at least 3 mixing components. Trace element data for Mauna Kea lavas are from this paper, and delta $^{208}Pb/^{204}Pb$ is calculated from Pb isotopic data in Blichert-Toft et al. (submitted manuscript, 2002). Field for Loihi lavas is from *Garcia et al.* [1993, 1998] and *Norman and Garcia* [1999].

tems 2002). A plot of $^{3}He/^{4}He$ versus delta $^{208}Pb/^{204}Pb$ (see Kurz et al., submitted manuscript, 2002, Figure 7) shows that for He and Pb isotopes these lavas trend toward the field of lavas from Loihi Seamount (also see Figure 11a). Based on SiO_2 content, Nb/Zr and $^{3}He/^{4}He$, *Rhodes* [2000] and *Kurz and Curtice* [2000] were the first to note the similarity of these Mauna Kea lavas to lavas from Loihi Seamount. In addition to high Nb/Zr (Figure 10f), high Ti/Zr is typical of some Loihi lavas (Figure 10g). Therefore, we conclude that samples of the Low SiO_2 Shield Group with the lowest $^{206}Pb/^{204}Pb$ and highest Nb/Zr and Ti/Zr contain the largest proportion of a Loihi-type component (Figures 10f, 10g, and 11a).

3.6. Abundance Ratios Involving Elements of Similar Incompatibility

[28] Each of the abundance ratios Nb/La, Nb/Ta, Nb/Th, Nb/U, Zr/Hf and Ce/Pb involve elements with similar geochemical characteristics. These ratios are not highly variable in oceanic basalt; typically they vary by less than a factor of two. However, numerous recent studies have shown that significant variations in these ratios are found in mid-ocean ridge and oceanic island basalt. These variations are inferred to reflect magmatic processes, specifically differences in partition coefficients, e.g., $D_{Hf} > 2D_{Zr}$ for clinopyroxene/melt [*Blundy et al.*, 1998]. However, these ratios in the Phase 2 core are typical for ocean island basalt and there are few significant differences between the Postshield and Shield groups (Figure 12).

3.6.1. Nb/Th

[29] The mean Nb/Th for the Phase 2 reference suite is 15.4 ± 1.4 (in this section the ± value indicates two standard deviations), very similar to that for the Phase 1 core (15.0 ± 3.6 and 16.2 ± 2.4 [*Albarede*, 1996; *Hofmann and Jochum*, 1996, respectively]), for postshield lavas on the subaerial slopes of Mauna Kea (14.3, [*Kennedy et al.*, 1991]) and to the average (15.2 ± 1.7) reported for Hawaiian shield basalt by *Hofmann* [1986]. It is notable that the Nb/Th ratio is greater than the primitive mantle estimate (8.6 [*Sun and McDonough*, 1989]), but to date there is no indication that Nb/Th is a useful discriminant for the different components contributing to Hawaiian volcanism.

3.6.2. Nb/U

[30] The mean Nb/U for the two groups of shield lavas is 45 ± 10, well within the global average of 47 ± 10 for oceanic basalt [*Hofmann*, 1986], and similar to that for the Phase 1 core (48 ± 12 and 53 ± 14 in *Albarede* [1996] and *Hofmann and Jochum* [1996], respectively). The Postshield lavas range to higher Nb/U, but given the similarity of Nb/Th in all groups, the higher Nb/U in upper lavas probably reflects U loss during postmagmatic alteration as proposed by *Kennedy et al.* [1991] for postshield lavas erupted on the high rainfall east flank of Mauna Kea. In the Phase 2 core, sample SR129 has the highest Nb/U (74), and its altered nature is indicated in Figure 4a.

3.6.3. Nb/Ta

[31] The average Nb/Ta of the shield lavas is 13 ± 2, similar to that reported for the Phase 1 core (12 ± 6 [*Albarede*, 1996]) and close to that for average MORB and OIB (16.7 ± 1.8 and 17.1 ± 2, respectively [*Kamber and Collerson*, 2000]). The highest Nb/Ta (up to 15.7 in SR125) occurs in the youngest postshield lavas. The slightly lower Nb/Ta of Phase 2 samples compared to OIB and MORB probably reflects Ta contamination arising from use of a WC shatterbox (see *Rhodes* [1996] for description of sample preparation for Phase 1 and 2 reference suite). Surprisingly Phase 1 Mauna Kea samples analyzed by *Albarede* [1996] range to much lower Nb/Ta of 2 to 3, hence the large standard deviation. Apparently, the samples of *Albarede* [1996] were contaminated by Ta.

3.6.4. Nb/La

[32] There is a general trend, with considerable scatter, for Nb/La to decrease upwards in the HSDP core (Figure 12). The mean value of 1.19 ± 0.10 of the Phase 2 data overlaps with the Phase 1 mean (1.18 ± 0.24 and 1.19 ± 0.08 in *Albarede* [1996] and *Yang et al.* [1996], respec-

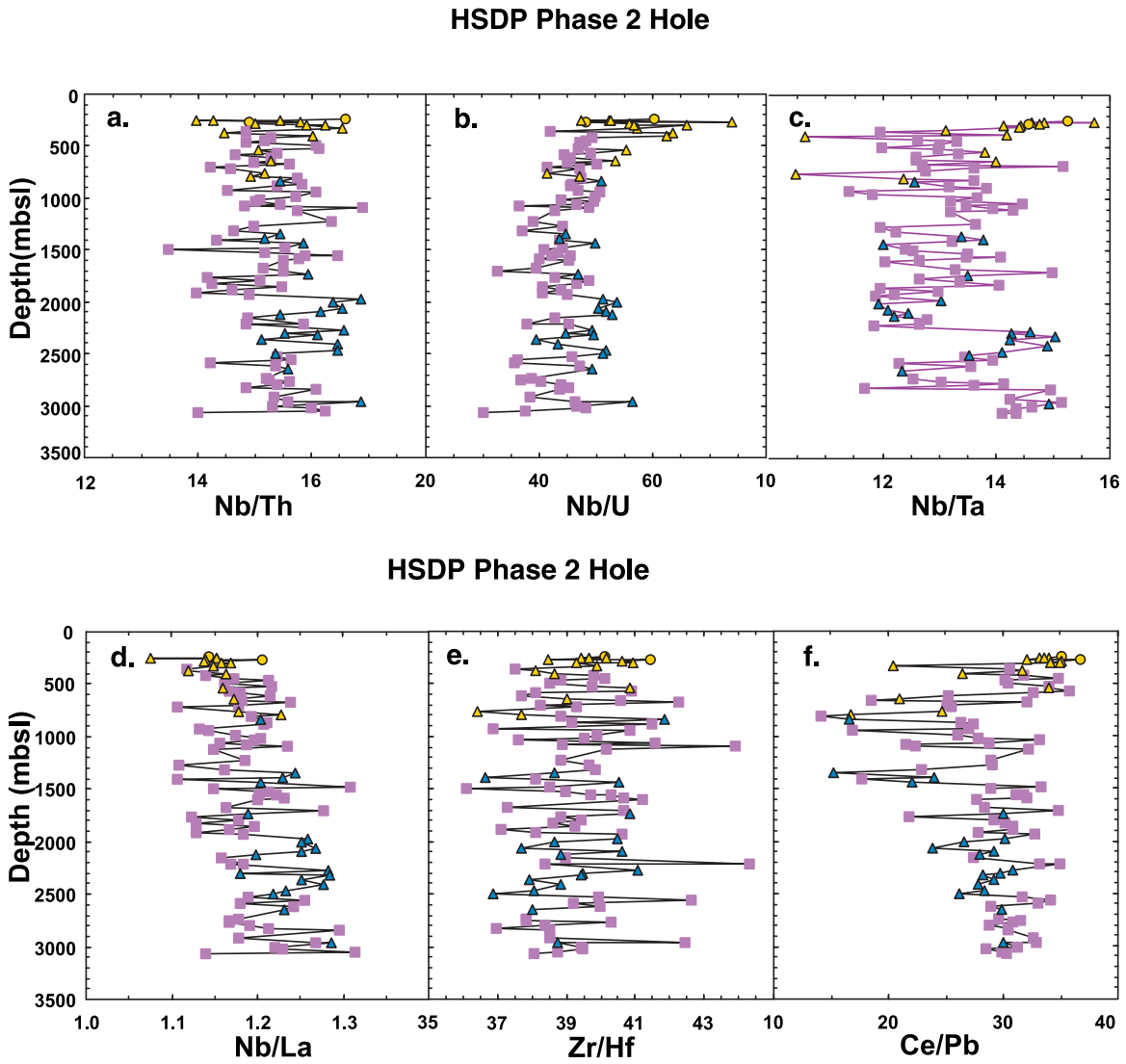

Figure 12. Abundance ratios of Nb/Th, Nb/U, Nb/Ta, Nb/La, Zr/Hf, and Ce/Pb versus depth in the Phase 2 core. All of these ratios involve highly incompatible elements or elements with similar geochemical characteristics (charge and ionic radius). Symbols as defined in Figure 8. There is no distinction between the two Shield Groups. There is a slight tendency for Postshield lavas to have relatively low Nb/La, and high Nb/U, Ce/Pb and Nb/Ta. The greater dispersion of Ce/Pb may reflect Pb contamination whereas that of Nb/U may reflect U mobility during alteration.

tively). All of these values exceed that of the primitive mantle estimate of 1.04 [*Sun and McDonough*, 1989]. Like Nb/Zr, the Nb/La ratio of Hawaiian shield lavas is correlated with radiogenic isotopic ratios (see subsequent discussion in section 4).

3.6.5. Zr/Hf

[33] The Zr/Hf ratio does not vary systematically with depth in the core and the mean value, 39 ± 3, is within the range for primitive OIB ~37 to 44 [*David et al.*, 2000] and similar to that for the Phase 1 core (42 ± 2 [*Yang et al.*, 1996]).

3.6.6. Ce/Pb

[34] Similarly, Ce/Pb does not vary with depth in the core and the mean 29 ± 8 (excluding two samples with anomalously high Pb content, see Figure 3) is similar to that typical of oceanic basalt (25 ± 5 [*Hofmann et al.*, 1986]). The range to low Ce/Pb (<20 in a few HSDP samples may reflect Pb contamination, but the lowest Ce/Pb occur over the

depth interval from ~300 to 1300 m. Possibly this is a zone of Pb mobility, but it does not overlap with the uppermost lavas with high Nb/U. The Ce/Pb ratios in the Phase 2 core are lower than the 40 ± 4 reported by *Kennedy et al.* [1991] for postshield Mauna Kea lavas but similar to the Phase 1 average (33 ± 8 and 40 ± 11 in *Albarede* [1996] and *Yang et al.* [1996], respectively).

3.7. Implications of Temporal Geochemical Trends in HSDP Cores

[35] In summary, the temporal geochemical trends defined by Mauna Kea lavas in the HSDP cores lead to the following conclusions.

[36] 1. HSDP lavas show that at Mauna Kea volcano there was a gradual and prolonged transition from shield- to postshield-stage volcanism commencing at ~370 ka (sample SR 340), and entering a phase of intercalated tholeiitic and alkalic basalt at ~230 ka (SR 131, Table 2). Studies of subaerially exposed Mauna Kea lavas show that postshield basaltic volcanism (Hamakua Volcanics) continued until 70–65 ka and was followed by a hawaiitic substage (Laupahoehoe Volcanics) erupted from 65–4 ka [*Frey et al.*, 1990, 1991; *Wolfe et al.*, 1997]. Although the HSDP postshield lavas are not highly evolved (MgO > 6.3%), they, in general, are more evolved than the underlying shield lavas, thereby providing evidence for increased crystal fractionation resulting from a decreasing magma supply to the crust, an inference that is consistent with the long time interval represented by these lavas (Figure 7f).

[37] Within the intercalated tholeiitic and alkalic basalt of the postshield-stage, the alkalic basalt does not have distinctive isotopic characteristics (Figure 8); hence we infer that low SiO_2 content and incompatible element enrichment of alkalic basalt was, at least in part, controlled by process. Specifically, we conclude that the uppermost HSDP lavas in the Mauna Kea section, the Postshield Group including intercalated alkalic and tholeiitic basalt, segregated at a lower extent of melting and higher pressure, within the stability field of garnet, than the underlying Mauna Kea lavas. Similar inferences were made from studies of the Phase 1 core [*Yang et al.*, 1996] and onland sections of Mauna Kea basalt [*Frey et al.*, 1991]. In addition the source of the Postshield Group had lower $^{3}He/^{4}He$ and less radiogenic Pb isotope ratios than older shield lavas. Similar results were obtained for the HSDP Phase 1 core [*Kurz et al.*, 1996; *Lassiter et al.*, 1996] and for other Hawaiian shields, such as Haleakala [*Kurz et al.*, 1987; *Chen et al.*, 1991]. Hence as a Hawaiian volcano migrates away from the hot spot, shield-stage volcanism wanes, extent of melting decreases, depth of melt segregation increases, magma supply to the crust decreases, crystal fractionation within the crust is enhanced, and there is an increased role for a depleted component with typically lower $^{3}He/^{4}He$ and $^{87}Sr/^{86}Sr$, higher $^{143}Nd/^{144}Nd$ and $^{176}Hf/^{177}Hf$ and less radiogenic Pb. In detail the trend to lower ε_{Hf} for the Postshield Group (Figure 8c) is anomalous.

[38] *Lassiter et al.* [1996, Figure 9] interpreted results for the Phase I core as reflecting a thermally and geochemically zoned plume. As the volcano moves over the relatively cool and depleted plume margin, melting extent decreases, melt segregation occurs at relatively higher pressure and partial melts have isotopic characteristics reflecting a role for a depleted source; i.e., relatively low $^{3}He/^{4}He$ and non-radiogenic Pb. The geochemical data for the Postshield Group of the Phase 2 core are consistent with this interpretation.

[39] 2. A new conclusion inferred from the lower part of the HSDP 2 core, deeper than 800 m, is that the Low SiO_2 Shield Group sampled a source whose partial melting led to relatively low SiO_2 content, relatively uniform La/Yb, relatively high Nb/Zr and Ti/Zr, high $^{3}He/^{4}He$ and high $^{208}Pb/^{204}Pb$ at a given $^{206}Pb/^{204}Pb$ (i.e., high delta $^{208}Pb/^{204}Pb$). This group cannot be distinguished on the basis of Sr, Nd or Hf isotopes or specific incompatible element abundance ratios, such as La/Yb and Nb/Zr. However, distinctive trends are defined by this group in ratio-ratio plots, such as Sm/Yb versus Nb/Zr and La/Yb versus Ti/Zr (Figures 10e and 10g); moreover, these ratios are correlated with delta $^{208}Pb/^{204}Pb$ (Figure 11). This Low SiO_2 Shield Group occurs throughout the core from ~800 to 3000 mbsl forming clusters of samples (e.g., the 3 subgroups formed by SR531–SR545–SR560, and SR732–SR741–SR750–SR756–SR762, and

SR791–SR796–SR800–SR814–SR826–SR836–SR842) which are intercalated with high SiO_2 lavas (Figures 7 and 8). In addition to relatively low SiO_2 content the two older subgroups (SR732 to SR762 and SR791 to SR842) are characterized by relatively high Nb/Zr and Ti/Zr (Figures 10d and 10e) and high $^3He/^4He$ and delta $^{208}Pb/^{204}Pb$ (Figures 8a and 8f). These are characteristics of lavas from Loihi seamount. This is a surprising result because it requires that volcanoes on both the Loa (Loihi) and Kea (Mauna Kea) trends [e.g., *DePaolo et al.*, 2001] sampled similar source materials early in their evolution. If this Loihi component is associated with the core of the Hawaiian plume, the conclusion of *Lassiter et al.* [1996, Figure 10] that Mauna Kea volcano sampled only the relatively cool peripheral part of the plume thereby bypassing the central part of the hot spot (plume source) is incorrect. However, if sample SR354, a relatively young (380 ka) subaerially erupted sample, also sampled the Loihi component, as we infer by including it in the Low SiO_2 Shield Group (Figure 8), this component contributed to the growth of Mauna Kea for 200 ka.

[40] 3. Despite the complexities arising from the role of geochemically distinct source components, the well-defined positive correlations between abundances of incompatible elements (Figure 3) show that these source components were not markedly different in abundance ratios involving highly incompatible elements (Figure 12).

4. Discussion: Comparisons of Hawaiian Shields

4.1. Intershield Differences in Abundance Ratios Involving Nb and Correlations With Radiogenic Isotope Ratios

[41] Like Mauna Kea samples in the HSDP core, lavas from different Hawaiian shields define positive trends between La/Yb and Nb/Zr, but the Koolau shield is offset to lower Nb/Zr (Figure 13a); this offset is much larger than Nb/Zr differences between groups within the Mauna Kea part of the HSDP cores. We infer that correlations between La/Yb and Nb/Zr reflect differences in extent of melting whereas intershield differences in these ratios reflect source heterogeneity. For example the La/Yb-Nb/Zr variation in HSDP postshield lavas is inferred to reflect varying extents of melting (Figure 10a), and relatively low extent of melting is also the likely explanation for the alkalic

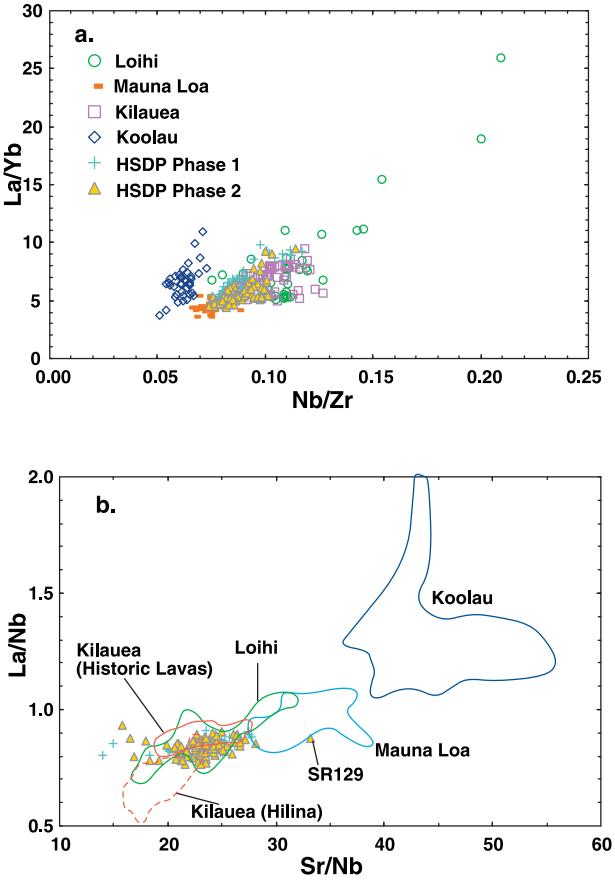

Figure 13. (a) La/Yb versus Nb/Zr for several Hawaiian shields. Although within shields these ratios are correlated, the Koolau shield lavas are offset to low Nb/Zr. Loihi alkalic lavas extend to the highest La/Yb and Nb/Zr, presumably reflecting a relatively low extent of melting [*Frey and Clague*, 1983; *Garcia et al.*, 1993]. (b) La/Nb versus Sr/Nb for several Hawaiian shields. Compared to La/Yb and Nb/Zr these ratios are less sensitive to variations in extent of melting. The shields define a positive trend with Mauna Loa and especially Koolau showing a relative Nb depletion, i.e, high La/Nb and Sr/Nb. The fields for Mauna Kea, Kilauea and Loihi overlap. Data sources: HSDP 1 [*Yang et al.*, 1996; *Rhodes*, 1996]; HSDP 2 (this paper); Koolau [*Frey et al.*, 1994; *Jackson et al.*, 1999; Huang and Frey, unpublished data, 2003], Mauna Loa [*Rhodes*, 1995; *Rhodes and Hart*, 1995; *Kurz et al.*, 1995; *Cohen et al.*, 1996]; Loihi [*Frey and Clague*, 1983; *Garcia et al.*, 1993, 1998; *Norman and Garcia*, 1998]; Kilauea (historic from *Pietruszka and Garcia* [1999]; Hilina from *Chen et al.* [1996]).

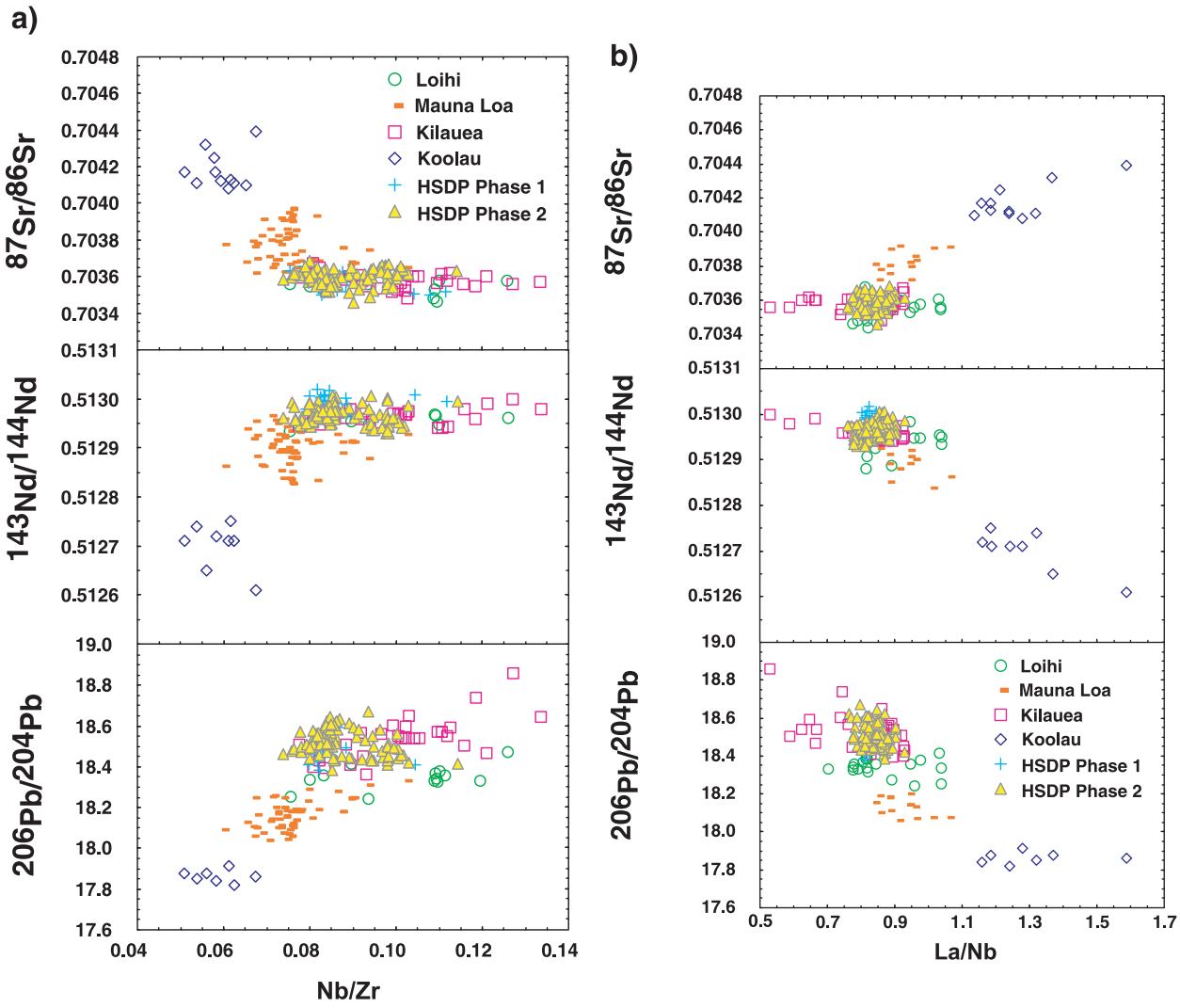

Figure 14. (a,b,c) Correlations of Nb/Zr, La/Nb and Ba/Th with isotopic ratios of Sr, Nd and Pb in the HSDP core and other Hawaiian shields. Inset in "c" shows that the distinctive geochemical groups for HSDP Mauna Kea lavas overlap in Ba/Th. Data Sources: HSDP 2 (this paper; Bryce and DePaolo, submitted manuscript, 2002; Blichert-Toft et al., submitted manuscript, 2002); HSDP 1 [*Rhodes*, 1996; *Lassiter et al.*, 1996]; Koolau [*Roden et al.*, 1994 and Huang and Frey, unpublished data, 2003]; Mauna Loa [*Rhodes and Hart*, 1995; *Kurz et al.*, 1995; *Cohen et al.*, 1996]; Loihi [*Garcia et al.*, 1993, 1995, 1998; *Norman and Garcia*, 1998]; Kilauea [*Chen et al.*, 1996; *Pietruszka and Garcia*, 1999].

lavas from Loihi seamount that range to high La/Yb and Nb/Zr (Figure 13a). In contrast, the relatively low Nb/Zr and high La/Nb (a ratio that is less sensitive than Nb/Zr to variations in extent of melting) of Koolau shield lavas is inferred to reflect source differences (Figure 13). Although the Low SiO_2 Shield Group at Mauna Kea is not distinct in La/Nb (Figure 12), we infer that their high Nb/Zr also reflects source control (Figures 10a and 10b).

[42] It is well established for Hawaiian shield lavas that incompatible element abundance ratios involving Nb correlate with radiogenic isotopic ratios [*Frey and Rhodes*, 1993; *Roden et al.*, 1994; *Yang et al.*, 1994; *Rhodes and Hart*, 1995, *Chen et al.*, 1996]. Such correlations provide the opportunity to identify compositional characteristics of the different source components contributing to Hawaiian lavas. Two ratios which provide good correlations with isotopic ratios are Nb/Zr and La/Nb (Figures 14a and 14b). Clearly, lavas from Koolau and to a lesser extent Mauna Loa are deficient in Nb, and their lavas trend to relatively low $^{206}Pb/^{204}Pb$, $^{143}Nd/^{144}Nd$ and high $^{87}Sr/^{86}Sr$.

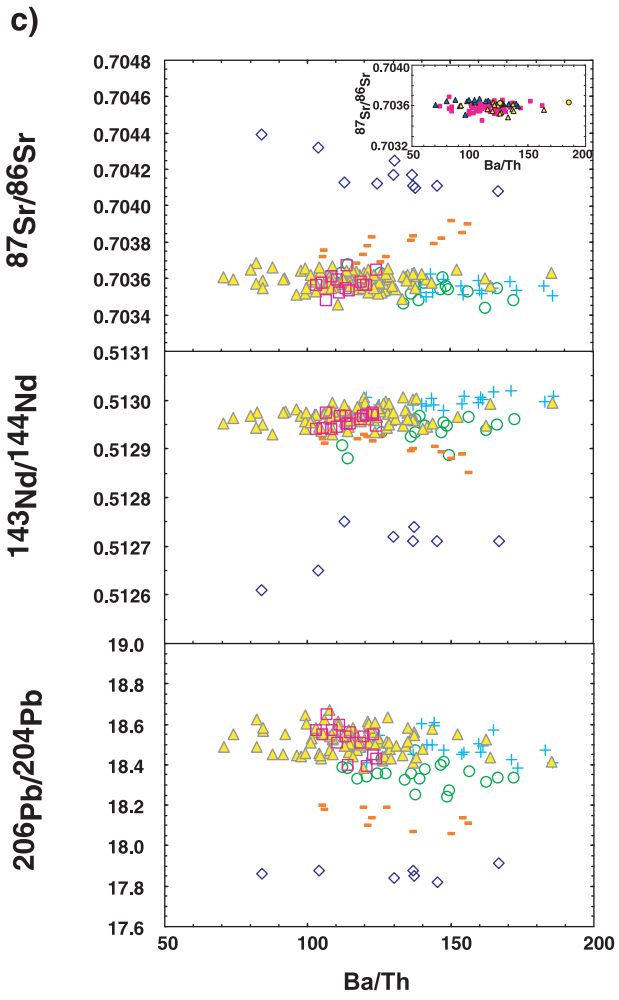

Figure 14. (continued)

Based on extrapolation of the intershield trends, the distinctive Koolau component has $^{206}Pb/^{204}Pb$ ~17.8 and $^{87}Sr/^{86}Sr$ ~0.7045 (Figure 14b). This constraint on $^{206}Pb/^{204}Pb$ is identical to that arising from the ε_{Hf} versus $^{206}Pb/^{204}Pb$ trend defined by Hawaiian shield lavas [see *Blichert-Toft et al.*, 1999, Figure 3]. In contrast, the Kea component defined by lavas from Mauna Kea and Kilauea has $^{87}Sr/^{86}Sr$ ~0.7036, $^{143}Nd/^{144}Nd$ ~0.5130 and $^{206}Pb/^{204}Pb$ ~18.6 (but see *Eisle et al.* [2002] for a discussion of Pb isotopic complexity in HSDP 2 lavas).

[43] It is also well known that abundance ratios involving Nb are strongly fractionated by the processes involved in arc magmatism. As a consequence, arc lavas and continental rocks have distinctly high La/Nb ratios [e.g., *Hofmann*, 1986]. Therefore, a plausible inference is that the relative deficiency of Nb in some Hawaiian shield lavas, such as Koolau lavas, reflects recycled source components derived from an arc tectonic setting. In addition to a Nb depletion, the Koolau component has high Pb/Hf, relatively high $^{18}O/^{16}O$, $^{87}Sr/^{86}Sr$, $^{187}Os/^{188}Os$, high $^{176}Hf/^{177}Hf$ for a given $^{143}Nd/^{144}Nd$ and relatively low $^{143}Nd/^{144}Nd$, $^{206}Pb/^{204}Pb$, $^{207}Pb/^{204}Pb$ and $^{208}Pb/^{204}Pb$ [*Roden et al.*, 1994; *Eiler et al.*, 1996; *Lassiter and Hauri*, 1998; *Blichert-Toft et al.*, 1999; *Jackson et al.*, 1999]. All of these geochemical characteristics are consistent with the conclusion that the distinctive Koolau component was derived from ancient recycled oceanic crust including pelagic sediment with a continental signature, i.e., relative depletion in Nb and enrichment in Pb [*Lassiter and Hauri*, 1998; *Blichert-Toft et al.*, 1999; *Jackson et al.*, 1999]. Although subduction zone processing must modify subducted oceanic crust, it is evident that in some cases important geochemical characteristics of at least some parts of subducted plates are recycled into the mantle and returned to the surface via plume-related volcanism. Moreover, the distinctive major element characteristics of Koolau shield lavas, notably high SiO_2/FeO and low CaO/Al_2O_3 [*Frey et al.*, 1994], can be explained by partial melting of a peridotite source that was refertilized by melts derived from recycled oceanic crust occurring as eclogite within peridotite [*Hauri*, 1996; *Green et al.*, 2001].

4.2. Abundance Ratios Involving Ba

[44] Abundance ratios involving Th, Ba, Nb and La are potentially useful in identifying components in the source of Hawaiian lava. These elements are highly incompatible in anhydrous phases; consequently, ratios such as Ba/Th, Ba/Nb and Ba/La in melts derived by >1% melting are equal to the source ratios. However, residues from partial melting will have ratios that differ significantly from those of the source. Also these ratios in melts are not very sensitive to fractional crystallization of anhydrous minerals, but cumulate phases, such as plagioclase, may have quite different ratios than the coexisting melts.

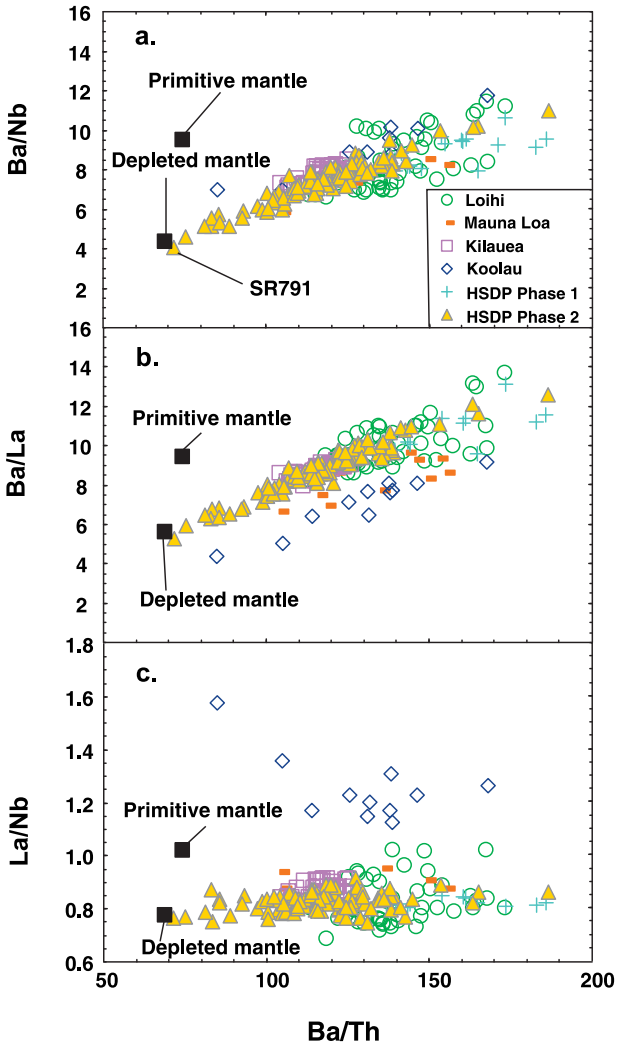

Figure 15. Abundance ratios involving highly incompatible elements: Ba/Nb, Ba/La and La/Nb versus Ba/Th for HSDP lavas and basalt from other Hawaiian shields. In the Ba/Nb-Ba/Th panel HSDP lavas and Hawaiian shields in general define a positive trend that extends toward depleted mantle (DM) estimates [*Hofmann*, 1988] but not toward primitive mantle (PM) estimates [*Sun and McDonough*, 1989]. A positive trend is also defined by Ba/La-Ba/Th, but basalt from the Koolau shield is offset to lower Ba/La at a given Ba/Th. In contrast to the more than a factor of two variation in Ba/Nb, Ba/La and Ba/Th, the La/Nb ratio is relatively constant, although Koolau lavas have high La/Nb at a given Ba/Th. Data sources are as given in Figure 13 caption.

[45] High Ba/Th (>100) relative to that of primitive mantle is characteristic of most Hawaiian shield lavas (Figure 15) [*Hofmann and Jochum*, 1996], melt inclusions within olivine phenocrysts in Mauna Loa lavas [*Sobolev et al.*, 2000] and even postshield- and rejuvenated-stage lavas [*Yang et al.*, 2003]. As shown by *Hofmann and Jochum* [1996], Ba/Th ratios in Hawaiian lavas are higher than those of MORB and most other ocean island basalt (Iceland is an exception [*Chauvel and Hemond*, 2000]). *Hofmann and Jochum* [1996] concluded that relatively high Ba/Th is characteristic of the present-day Hawaiian source and not a result of melting or postmelting processes; they proposed that the high Ba/Th signature results from an eclogite component in the source that formed as plagioclase-rich cumulate gabbro. Such a component is apparently ubiquitous in the source of Hawaiian lavas; an inference that contrasts with the localized presence of the component creating relative Nb deficiencies.

[46] If Ra/Th ratio is a proxy for Ba/Th, further insight into Ba/Th fractionation during the melting process creating Hawaiian tholeiitic basalt is provided by measurements of (^{226}Ra/^{230}Th) disequilibria; e.g., *Pietruszka et al.* [2001] found that the activity ratio (^{226}Ra/^{230}Th) is typically ~1.1 in historic tholeiitic basalt from Kilauea Volcano. This 10% disequilibrium can arise from the melting process (a consequence of different partition coefficients for Ra and Th), and from radiogenic ingrowth of ^{226}Ra during the melting process. Figure 7 of *Pietruszka et al.* [2001] shows that at very low extents of melting ($\ll$1%), ~10% disequilibrium results from the difference in partition coefficients. However, at the 5 to 10% extent of melting generally proposed for Kilauea lavas [e.g., *Pietruszka and Garcia*, 1999] most of the (^{226}Ra/^{230}Th) disequilibria results from radiogenic ingrowth. We conclude that Ra/Th and Ba/Th were not controlled by the melting process; therefore anomalously high Ba/Th is a characteristic of the source for Hawaiian lavas.

[47] Within the Phase 2 core, Ba/La, Ba/Nb and Ba/Th are quite variable but strongly correlated; these ratios vary by a factor of ~2.6 with one standard deviation of ~15% (Figure 16). In contrast to these ratios involving Ba, other ratios involving only highly incompatible elements, such as La/Nb, are much less variable, especially within a shield (Figures 15c and 16). Even the variability of several ratios involving elements with significant differences in their incompatibility (e.g., La/Sm, Sm/Yb

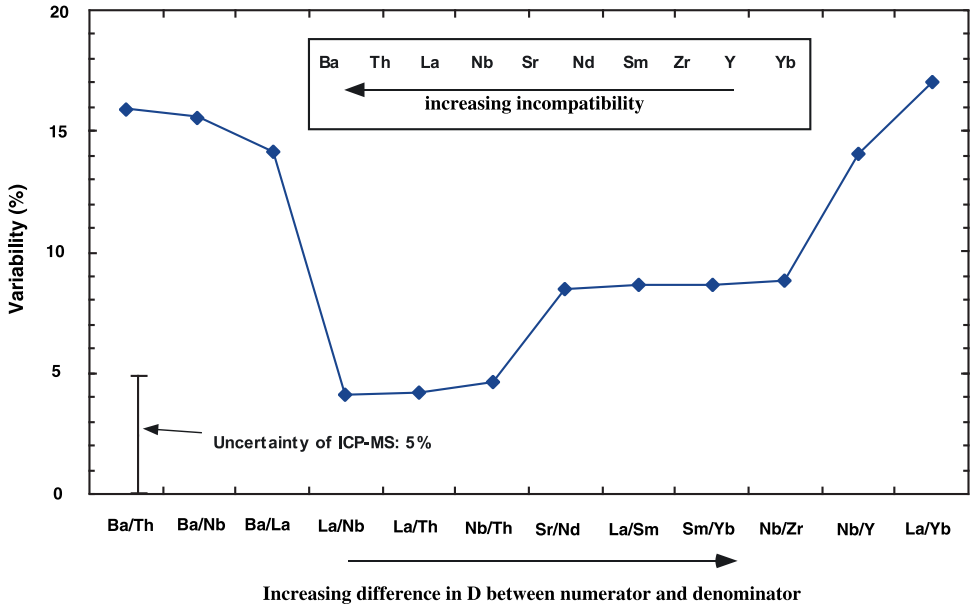

Figure 16. Variability [(one standard deviation/mean) × 100] in abundance ratios of incompatible elements in HSDP 2 lavas.

and Nb/Zr) is less than that of Ba/(La, Nb, Th) ratios; in fact, the ranges for Ba/La, Ba/Nb and Ba/Th are similar to that found for Nb/Y and La/Yb, ratios involving elements of very different incompatability (Figure 16).

[48] If high Ba/Th is a source characteristic, we expect this ratio to correlate with radiogenic isotope ratios. Historic Kilauea lavas define an inverse trend for Ba/Th versus $^{206}Pb/^{204}Pb$ and Mauna Loa lavas (<30 ka) show correlations of Ba/Th with Sr, Nd and Pb isotopic ratios (Figure 14c). However, in older and more altered lavas, e.g., from the HSDP cores and Koolau shield, Ba/Th ratios are considerably more variable than in lavas from Kilauea and Mauna Loa (Figure 15). Analyses of 101 Phase 1 HSDP Mauna Kea samples (not the reference suite) by *Albarede* [1996] showed that for the lower parts of the Phase 1 core (689 to 1041 m) ratios of Rb/Th, Cs/Th and to a lesser extent Ba/Th decrease upwards in the core. A Principal Component Analysis of the data showed that a component, accounting for 5.1% of the variance, has maximum loading on Rb and Cs, moderate loading on Ba and marginal loading on U [*Albarede*, 1996]. Given the well-documented postmagmatic mobility of Rb, Cs, and U, a plausible inference is that relatively low Ba/Th reflects Ba loss and that the variable Ba/Th in the upper part of the Phase 1 core reflects lateral fluid (H_2O) advection [see *Albarede*, 1996, Figure 3]. In the Phase 2 core Ba/Th ranges from 70 to 185, but there is no correlation with depth or compositional group (see inset in Figure 14c). To determine the effects of postmagmatic processes on Ba abundance in the Phase 2 core, Huang, Vollinger, Frey and Rhodes are determining compositional variations within four flow units. Based on data for 6 to 7 samples from these units, we find that Ba is not correlated with K. This result is consistent with the lack of correlation between K_2O/P_2O_5 and Ba/Th in the reference suite of samples. Nevertheless, variable Ba abundance at nearly constant Th content within individual units leads us to conclude that some of the Ba/Th variability in the Phase 2 core arises from postmagmatic alteration. Because there is evidence for both loss and addition of Ba, we infer that the extremes of Ba/Th (<100 and >150) may reflect alteration.

[49] In summary the data arrays in Figure 14c could be explained by mixing of components with distinct combinations of Ba/Th and isotopic ratios. Particularly important are the diverse Ba/Th versus $^{87}Sr/^{86}Sr$ and $^{143}Nd/^{144}Nd$ trends defined by Koolau and Mauna Loa lavas. If these trends reflect magmatic characteristics, they convey important information about source components. However, Koolau

Table A1a. Isotopes Analyzed by ICP-MS at MIT

Element	Isotope
Sc	45
Cr	53
Ni	61
Ni	62
Se	77
Rb	85
Sr	86
Y	89
Zr	91
Nb	93
In	115
Cs	133
Ba	135
Ba	137
La	139
Ce	140
Pr	141
Nd	143
Nd	145
Sm	147
Sm	149
Eu	151
Sm	152
Eu	153
Tb	159
Gd	160
Dy	163
Ho	165
Er	167
Tm	169
Yb	174
Lu	175
Hf	178
Hf	179
Ta	181
Pb	206
Pb	208
Bi	209
Th	232
U	238

lavas (~2 to 3 Ma) are variably altered [*Frey et al.*, 1994], and it is necessary to determine if their systematic Ba/Th-isotope ratio trends in Figure 14c are a fortuitous combination of source heterogeneity (isotopic ratios) and alteration (Ba/Th).

5. Summary

[50] Based on study of Mauna Kea lavas in reference sample suites from the two HSDP cores we identify 3 major types of geochemically distinct magmas.

[51] 1. Lavas within the upper 150 m (<200 ka to ~330 ka) of the Mauna Kea section are low SiO_2 basalt with intercalated alkalic and tholeiitic basalt in the upper 50 m; these lavas form the Postshield Group. Their relatively low SiO_2 is coupled with high incompatible element content, and high La/Yb and Sm/Yb; hence, relative to underlying lavas they were derived by lower extents of melting and segregated at higher pressure within the stability field of garnet. Relative to underlying lavas they also contain more of a component with relatively low $^3He/^4He$, high ε_{Nd} and non-radiogenic Pb. These changes in process and source are interpreted to have occurred as the Mauna Kea shield passed over the periphery of the thermally and geochemically zoned plume.

Table A1b. MIT ICP-MS Typical Procedure[a]

Position	SOLUTION
1	EDM
2	STD
3	UNKNOWN
4	UNKNOWN
5	UNKNOWN
6	UNKNOWN
7	EDM
8	STD
9	UNKNOWN
10	UNKNOWN
11	UNKNOWN
12	UNKNOWN
13	EDM
14	STD
15	UNKNOWN
16	UNKNOWN
17	UNKNOWN
18	BLANK
19	EDM
20	STD
21	UNKNOWN
22	UNKNOWN
23	UNKNOWN
24	UNKNOWN
25	EDM
26	STD
27	UNKNOWN
28	UNKNOWN
29	UNKNOWN
30	UNKNOWN
31	EDM
32	STD
33	UNKNOWN
34	UNKNOWN
35	UNKNOWN
36	UNKNOWN
37	EDM

[a] Abbreviations are as follows: EDM, external drift monitor solution; STD, standard sample solution; BLANK, blank solution; UNKNOWN, unknown solution.

Table A2. Trace Element Abundances (ppm) in 3 USGS Standard Samples Used in ICP-MS at MIT

	AGV-1	BCR-1	BHVO-1
Rb	68	48	9.50
Sr	655	326	390
Y	21	39	27.6
Zr	227	190	179
Nb	14.5	12.5	19.0
Ba	1223	687	133
La	38	24.9	15.5
Ce	67	53.7	39.0
Pr	8.45	6.88	5.70
Nd	31.6	28.8	25.2
Sm	5.9	6.6	6.20
Eu	1.64	1.95	2.06
Gd	5	6.69	6.03
Tb	0.664	1.068	0.96
Dy	3.6	6.35	5.20
Ho	0.69	1.315	0.990
Er	1.856	3.7	2.40
Tm	0.34	0.56	0.330
Yb	1.644	3.35	2.02
Lu	0.248	0.505	0.278
Hf	5	4.97	4.38
Ta	0.9	0.81	1.23
Pb	36	13.5	2.10
Th	6.5	6.19	1.16
U	1.92	1.7	0.420

[52] 2. Deeper in the Phase 2 core, >800 mbsl, two other groups, presumably intrinsic to the plume, are intercalated. These shield lavas are distinguished by different SiO_2 contents at a given MgO content. Most of the HSDP Mauna Kea lavas belong to the relatively high SiO_2 group (~49–51% SiO_2 after adjusting lava composition to be in equilibrium with Fo_{85} olivine). This group defines the Kea component.

[53] 3. Like the Postshield Group, the other group is distinguished by a relatively low SiO_2 content (<48.8% after adjusting lava compositions to be in equilibrium with Fo_{85} olivine). Unlike the Postshield Group, this shield group has relatively high Nb/Zr, Ti/Zr and $^3He/^4He$ and high $^{208}Pb/^{204}Pb$ at a given $^{206}Pb/^{204}Pb$. These are the characteristics of tholeiitic lavas erupted at Loihi seamount. This geochemically distinctive component contributes to early shield volcanism at both Kea and Loa trend volcanoes. Based on abundance ratios such as La/Yb, Sm/Yb and Nb/Zr this group did not segregate within the garnet stability field.

[54] 4. Although in detail the HSDP cores contain distinctive geochemical groups of lavas, within the context of all Hawaiian shields Mauna Kea shield lavas are not highly heterogeneous in isotopic ratios of Sr, Nd and Hf or in La/Nb and Nb/Zr. Ratios involving Nb reflect the Koolau component (recycled oceanic crust including pelagic sediment), and there is no evidence for this component in Mauna Kea lavas. Like other Hawaiian lavas, Mauna Kea lavas have high Ba/Th (>100), but this ratio is highly variable, possibly a result of alteration, and it is not correlated with radiogenic isotope ratios.

Appendix A: Analytical Procedures

A1. Instrumental Neutron Activation Analysis (INAA)

[55] Determination of Na, Cr, Sc, La, Ce, Nd, Sm, Eu, Tb, Yb, Lu, Hf and Th abundances by INAA followed the procedures of *Ila and Frey* [1984,

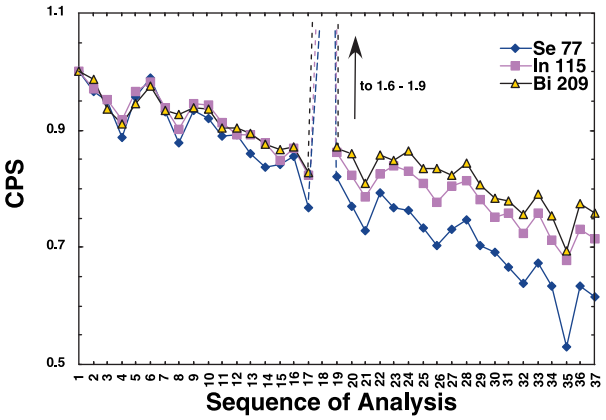

Figure A1. Sensitivity drift in internal drift monitors. Counts per second (CPS) normalized by the isotope concentrations in the solutions, and then normalized to CPS of the first external drift monitor (EDM), for the 3 internal drift monitors (^{77}Se, ^{115}In, ^{203}Bi) in a sequence of solutions, 1 to 37, analyzed over 6 hours. Generally, the statistical uncertainty in CPS is less than 3% (2σ). The non-uniform behavior of the 3 isotopes indicates that sensitivity drift is a function of time and mass. Because the sensitivity drift is a complicated function of mass, use of only 3 isotopes does not adequately correct for drift as a function of mass (See Figure A2). Solution 18 in the sequence is a blank solution (i.e., it contains only the internal drift monitors and acid.). It has very high CPS because of the absence of a dissolved rock matrix which depresses the signal strength.

2000]. The accuracy and precision of this procedure for analyses of Hawaiian basalt are documented in *Frey et al.* [1990, Table 1d] and for HSDP 1 samples in *Yang et al.* [1996, Table 1]. Also analyses of USGS standards are reported in *Ila and Frey* [2000]; BHVO-2 data are in Table A3.

A2. Inductively Coupled Plasma Mass Spectrometry (ICP-MS)

A2.1. Sample Dissolution

[56] Samples were dissolved using a HF-HNO_3 multistage digestion procedure in Teflon Savillex beakers. Rock powder, 50 to 100 mg, was weighed into a precleaned Teflon Savillex beaker; then 2 mL concentrated HF and 0.5 mL 14M HNO_3 were added. The mixture of acids and rock powder in uncapped beakers was dried at 350°F to form a moist sample cake. Then 3.5 mL concentrated HF and 0.5 mL of 7M HNO_3 were added to this sample cake. The capped beaker was heated at 250°F for 3 to 5 days. Then the sample was dried at 350°F to form a thick liquid gel, and 5 mL of 7M HNO_3 were added. Again the sample was dried at 350°F to form a moist cake, and 5 mL of 7M HNO_3 were added. Then the capped beaker was heated at 250°F overnight. Approximately 10% of the samples were not totally dissolved at this stage. These samples were transferred to a Teflon bomb and the same procedure outlined above was followed. The bomb treatment was repeated until the sample was totally dissolved. The samples were then diluted by a factor of 2000 to 8000 using 1M HNO_3 and spiked with a solution, containing three isotopes, ^{77}Se, ^{115}In and ^{209}Bi, with known concentrations prior to aspiration into a Fissons (VG) Plasmaquad 2+S ICP-MS.

A2.2 Analytical Procedure

[57] Our procedure typically involves sequential analysis of 37 sample solutions over a ~6 hour time span. One to three isotopes are selected for each element based on high natural abundances and no or minimal isobaric and oxide interferences (Table A1a). Data are collected and reported as count rates (counts per second or "CPS") for these isotopes. We use a standard calibration curve to convert these ion count rates into elemental abundances. Several USGS standard samples, BHVO-1, BCR-1 and AGV-1, are used to obtain the standard calibration curve (Table A2). The sensitivity of the instrument at a given mass is not stable with time. In addition, this temporal fluctuation in signal strength varies with isotope mass. These mass- and time-dependent variations are described as "sensitivity drift" (Figure A1).

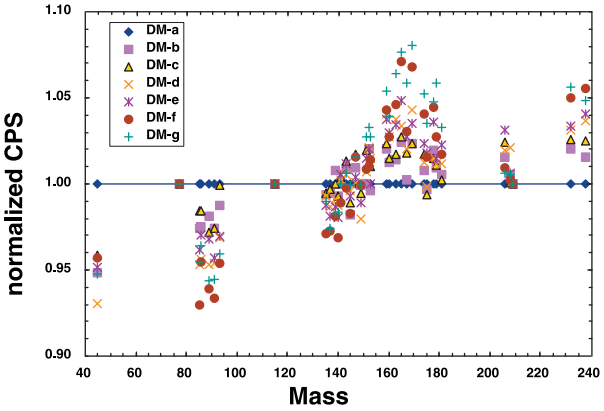

Figure A2. Sensitivity drift in external drift monitors. CPS (normalized by their isotope concentrations in the solutions), after applying the internal drift correction factor (IDF), normalized by CPS of the first external drift monitor, in 7 external drift monitors for all the analyzed isotopes. The 7 external drift monitors were run in the order of DM-a, DM-b, DM-c, DM-d, DM-e, DM-f, DM-g. Notice that after applying the IDF, the normalized CPS do not define a horizontal line at unity. However, the shapes of IDF corrected CPS in EDMs, relatively low at lower mass and high at higher mass, are similar for each EDM. Clearly, the internal drift correction has not sufficiently corrected for sensitivity drift as a function of mass.

[58] In order to correct for sensitivity drift, both internal and external drift monitors are used. Three spiked isotopes, ^{77}Se, ^{115}In and ^{209}Bi, are used as internal drift monitors (IDM). They record the sensitivity drift for these three isotopes in every analyzed solution. Beginning with the first solution in the analytical procedure, every sixth solution is an identical solution, such as BHVO-1, known as the external drift monitor (EDM). We use these EDMs to record the sensitivity drift in all the analyzed isotopes. Table A1b shows the typical sequence of analysis: external drift monitor, standard sample solution, 4 unknown solutions, etc.

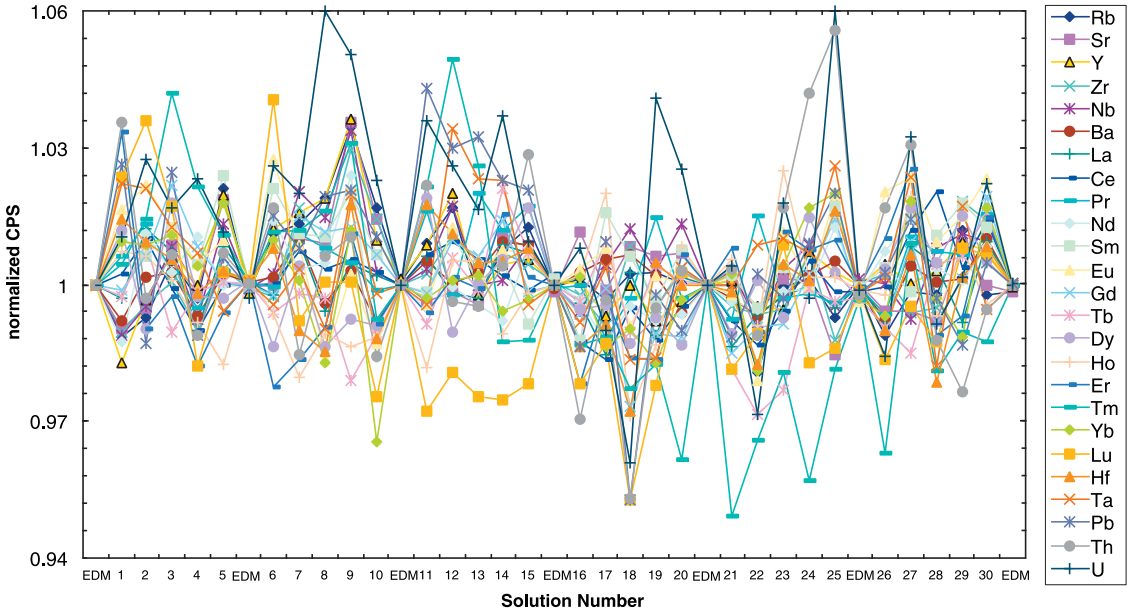

Figure A3. Normalized CPS in 37 solutions of BHVO-1 for 25 elements. Both internal drift correction factor (IDF) and external drift Correction Factor (EDF) were applied following the procedure described in the text. Solutions labeled as EDM are external drift monitors which were normalized to the CPS of the first EDM in order to determine the EDF; therefore for each element in every EDM, the normalized CPS are unity. For solutions run between two EDM (Table A1b), the EDF was determined for each analyzed isotope using a cubic spline fit to the EDF for each EDM. Ideally, since all analyzed solutions are from the same solution of BHVO-1, the normalized CPS in all the solutions should be unity. The discrepancy from unity provides estimates of the uncertainty resulting from both the analytical technique and sensitivity drift correction procedures.

[59] Figure A1 shows the sensitivity drift in the three spiked isotopes, ^{77}Se, ^{115}In and ^{209}Bi, in all solutions during one analytical procedure (~6 hours). The first drift correction, the internal drift correction, is based on these 3 spiked isotopes. Since the concentrations of the three spiked isotopes are known in every solution, CPS for these three isotopes are first normalized by their isotope concentrations; then are normalized to CPS of the first EDM. Hence, for each of the three isotopes we have a correction factor for every solution. We call this the internal drift correction factor (IDF). We assign an IDF to each analyzed isotope mass using a linear interpolation (extrapolation for ^{232}Th, ^{238}U and ^{45}Sc).

[60] In most situations, the internal drift correction does not adequately correct the sensitivity drift for all analyzed isotopes; therefore, we also correct for sensitivity drift using the external drift monitors. Figure A2 shows the sensitivity drift, after internal drift correction, in all the analyzed isotopes in EDMs during one procedure (~6 hours). Clearly, the range in internal drift corrected CPS from 0.92 to 1.08 (Figure A2) shows that internal drift correction has not adequately corrected the sensitivity drift. Therefore, we also apply an external drift correction. We normalize the CPS in all EDMs to that in the first one; hence, we have a correction factor for each of the analyzed isotopes in every external drift monitor. We call this the external drift correction factor (EDF). Because an external drift monitor is analyzed as every sixth solution in the analytical sequence (Table A1b), we must interpolate to determine the EDF for each intervening solutions, i.e. the 4 unknown and one standard solutions. This interpolation is done using a cubic spline fit. After application of the EDF, the reproducibility of all analyzed elements is better than ±6%, and better than ±3% for most of these elements. The only "cost" is that seven EDMs are analyzed (Table A1b), which increases machine time by 20%.

A3. Estimation of Precision and Accuracy

[61] Most of the uncertainty in ICP-MS data are caused by sensitivity drift during the analysis.

Table A3. Trace Element Abundances in BHVO-2 Analyzed by MIT ICP-MS and Other Techniques[a]

	MIT ICP-MS		MIT INAA		Lin et al. ICP-MS		Raczek et al.[b]		USGS Recommend	
	Mean of 11	Uncertainty (%)	Mean of 6	Uncertainty (%)	Mean of 6	Uncertainty (%)	Mean of 3	Uncertainty (%)	Mean	Uncertainty (%)
Rb	9.48	1			9.04	5.8	9.08	0.7	9.8	10
Sr	399	2			399	3.1	396	0.2	389	6
Y	28.3	2			25.6	5			26	8
Zr	178	1			170	4.7			172	6
Nb	19.0	1			18.2	4.7			18	11
Ba	135	2			134	4.5	131		130	10
La	15.2	2	14.8	2	15.1	2.7	15.2	0.4	15	7
Ce	38.4	1	38.8	1	37.6	4.6	37.5	0.3	38	5
Pr	5.57	1			5.13	1.2	5.29	0.9		
Nd	24.9	1	24.6	3	25.1	1	24.5		25.0	7
Sm	6.16	1	6.0	1	6.31	5.1	6.07	0.1	6.2	6
Eu	2.03	1	2.01	1	1.94	3.5	2.07	0.7		
Gd	6.13	2			5.76	6.1	6.24	0.4	6.3	3
Tb	0.963	2	0.88	5	0.9	3.3	0.936	1.7	0.9	
Dy	5.30	2			5.3	2	5.31	0.3		
Ho	1.01	2			1.05	2.7	0.972		1.04	4
Er	2.50	1			2.68	8.9	2.54	0.2		
Tm	0.350	3			0.35	7.1	0.341	2.3		
Yb	2.05	1	1.89	3	2.2	6	2.00	0.3	2	10
Lu	0.286	3	0.275	4	0.3	5.7	0.274		0.28	4
Hf	4.42	2	4.2	2	4.52	6.2			4.1	7
Ta	1.22	2	1.04	5	1.35	3.7			1.4	
Pb	1.53	2								
Th	1.30	3	1.06	2	1.2	12			1.2	25
U	0.446	2			0.45	10				

[a] Uncertainty = (1 σ/mean) × 100%.
[b] All element abundances were determined by ID-TIMS, except for Pr, Tb, Ho and Tm which were determined by MIC-SSMS.

Therefore, the sensitivity drift correction factors are very important in controlling the precision and accuracy of the data determined by ICP-MS. In order to evaluate our sensitivity drift correction procedure, we repeatedly analyzed a BHVO-1 solution using our typical analytical procedure, i.e., in this procedure all the unknown and standard sample solutions and EDMs are a BHVO-1 solution. In this experiment, after sensitivity drift corrections (IDF and EDF), all the solutions should have the same signal strength, i.e., the same CPS. For comparison, we normalized the CPS of all the solutions to that of the first solution. Figure A3 shows the normalized CPS values for each of the 25 analyzed elements. Overall, the normalized CPS values are within ±6% for all the solutions, most are within ±3%. The uncertainties, one standard deviation in percent, of these 25 elements are ~1–2%.

[62] In order to evaluate accuracy, we analyzed, BHVO-2, a newly prepared USGS standard sample. The average values and standard deviations of 11 replicate analyses obtained over ~5 months are reported in Table A3. For comparison, Table A3 also shows the trace element abundances in BHVO-2 reported by *Ila and Frey* [2000], *Lin et al.* [2000], *Raczek et al.* [2001] and the USGS recommended values. Except for Tb and Yb, the trace element abundances in BHVO-2 analyzed by ICP-MS at MIT are within ±5% of the INAA values reported by *Ila and Frey* [2000]. Values of Tb and Yb in BHVO-2 analyzed by MIT ICP-MS are about 8% higher than reported by *Ila and Frey* [2000]. Our reported values for BHVO-2 are also within ±5% of the values reported by *Raczek et al.* [2001], and for most of the elements the differences between the two reported values are within analytical uncertainties (Table A3). Taking the uncertainty into account, except for Gd and Y, our results are also in agreement with that reported by *Lin et al.* [2000]. Compared with the USGS recommended values, the difference between our

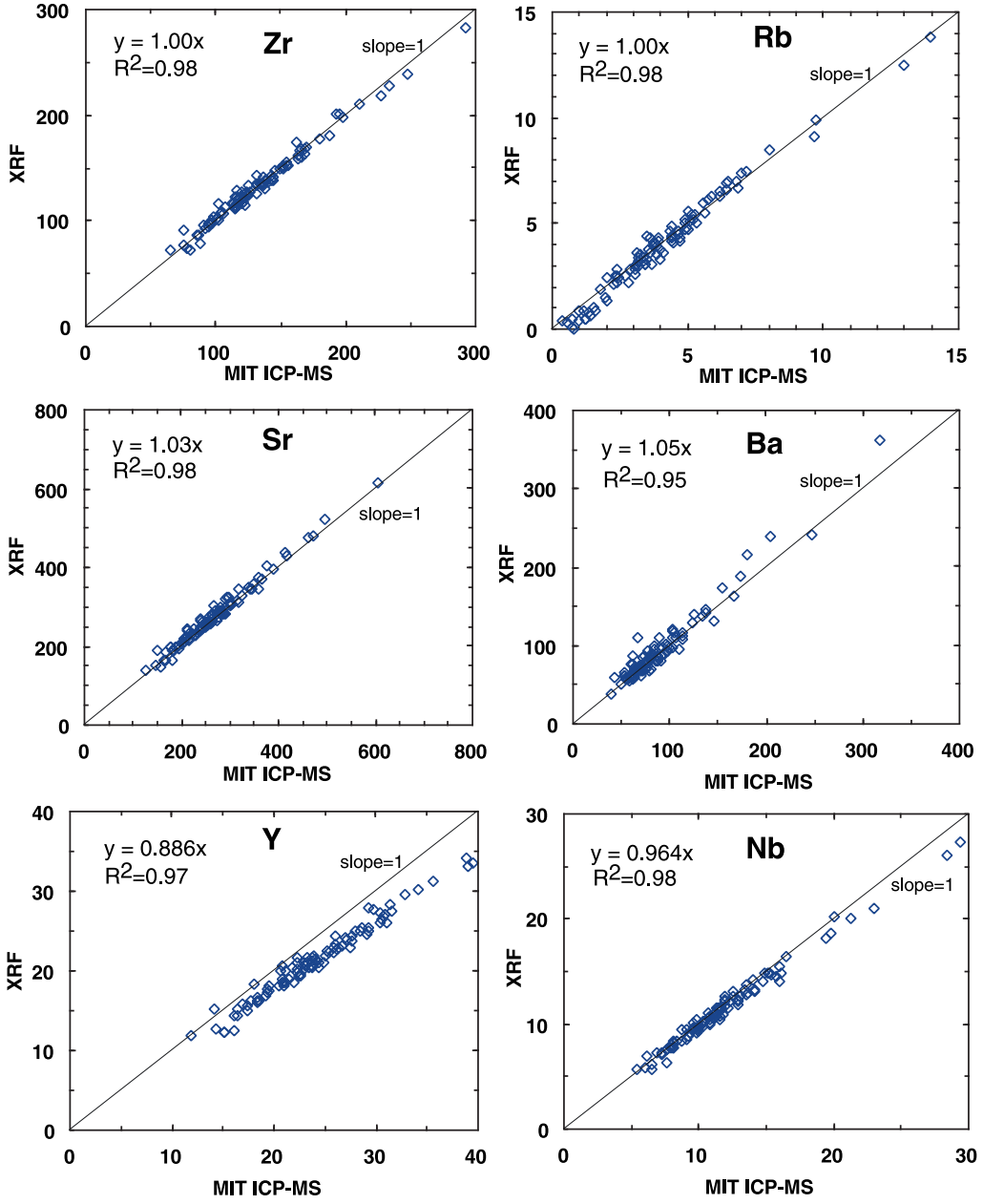

Figure A4. Comparisons between MIT ICP-MS and XRF. Comparisons between trace element abundances in HSDP-2 lavas obtained by ICP-MS at MIT (this paper) and XRF at UMASS (Rhodes and Vollinger, submitted manuscript, 2002). Regression equations are forced to intersect the origin. R^2 is linear correlation coefficient.

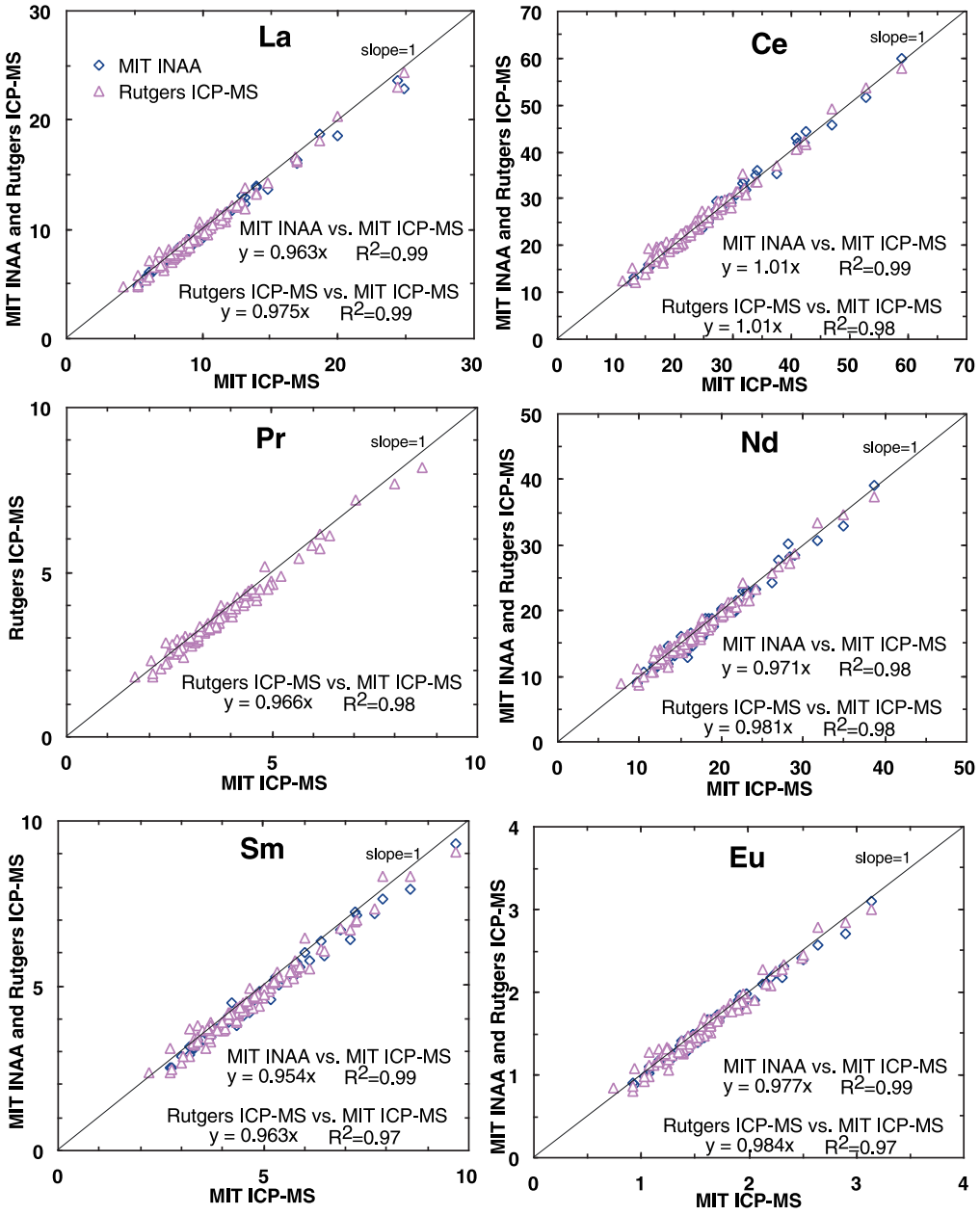

Figure A5. Comparison between ICP-MS and INAA. Comparisons between trace element abundances in HSDP 2 lavas obtained by ICP-MS at MIT (this paper), ICP MS at Rutgers (Feigenson et al., submitted manuscript, 2002) and INAA at MIT (this paper). Regression equations are forced to intersect the origin. R^2 is linear correlation coefficient.

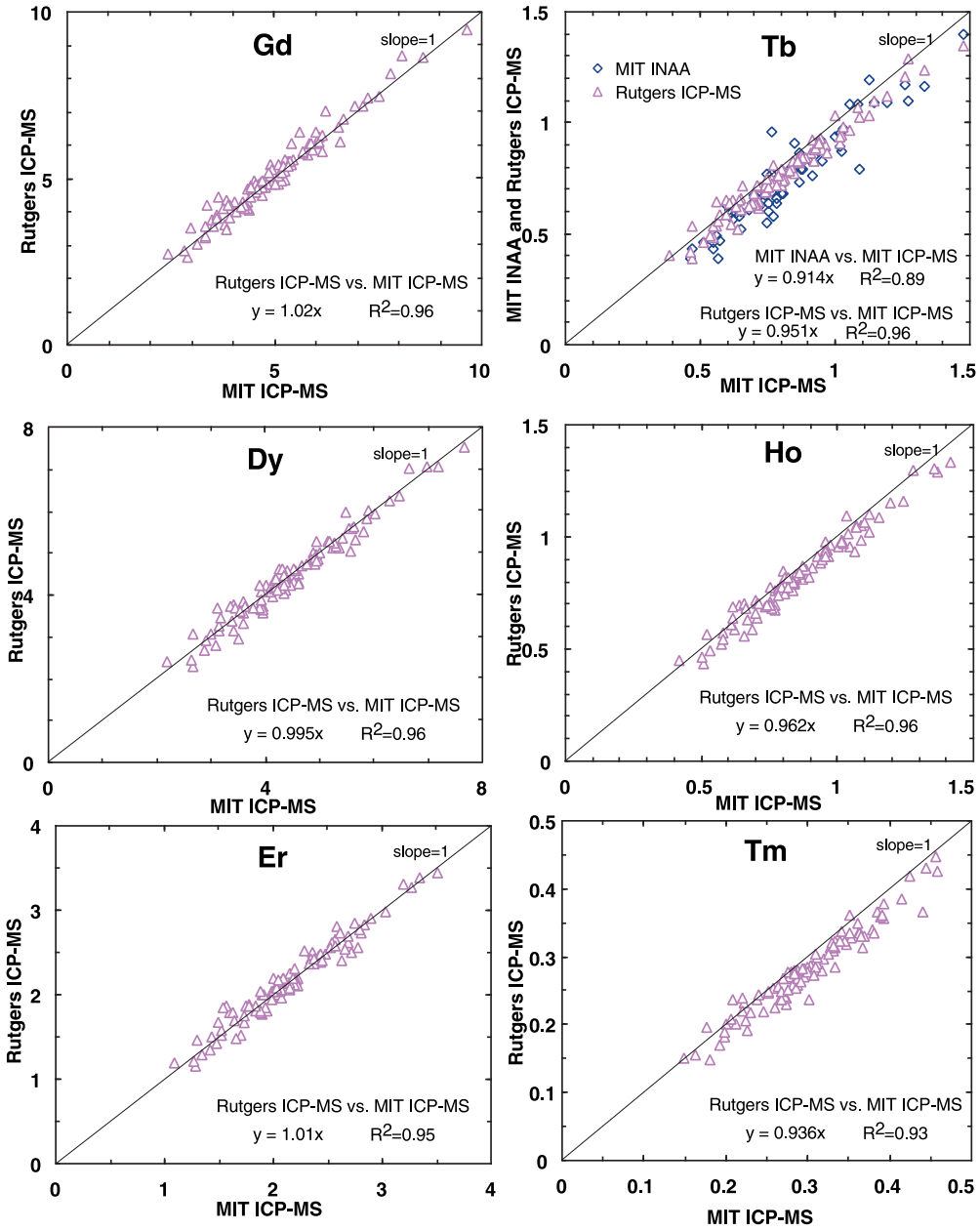

Figure A5. (continued)

reported values for BHVO-2 and the recommended values are within the reported standard deviations (Table A3).

A4. Comparison With Other Techniques (XRF and INAA) and Another ICP-MS Facility

[63] Trace element abundances for HSDP Phase 2 reference samples have also been determined by X-ray fluorescence (Rhodes and Vollinger, submitted manuscript, 2002), INAA at MIT (this paper) and ICP-MS at Rutgers (Feigenson et al., submitted manuscript, 2002). These multiple data sets for the same samples provide the opportunity for comparison of results obtained by different techniques or the same technique (ICP-MS) in different facilities.

A4.1 ICP-MS (MIT) Compared to XRF (University of Massachusetts)

[64] In Figure A4, we compare results obtained by ICP-MS (MIT) and XRF (Univ. Massachusetts).

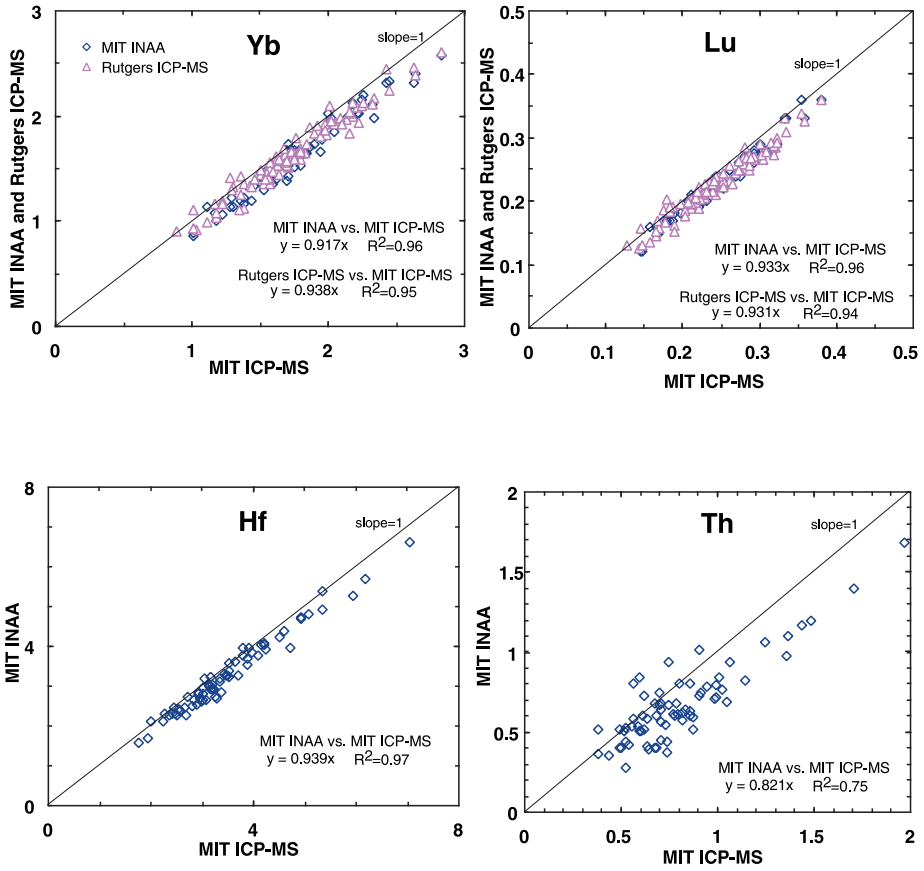

Figure A5. (continued)

The linear correlation coefficients between the two data sets for Ba, Sr, Zr, Nb, Rb and Y are greater than 0.95 (Figure 4). These results show that the precision of both techniques is comparable, ~3–6%, and the slopes are near unity for each element (except Y), thereby indicating that both analytical techniques yield similar abundances. However, for Y abundance there is a systematic difference between the two techniques with the Y abundance determined by ICP-MS approximately 12% higher than that determined by XRF.

A4.2. ICP-MS (MIT Compared to Rutgers)

[65] In Figure A5 we compare ICP-MS results for REE abundances obtained at MIT and Rutgers. For La, Ce, Pr, Nd, Sm and Eu the correlation coefficients are 0.98 to 0.99 and systematic differences are <4%. Correlation coefficients for Gd, Tb, Dy, Ho, Er, Tm, Yb and Lu are lower 0.93 to 0.96 and systematic differences are ≤5%, except for Tm, Yb and Lu whose abundances determined at MIT are 6 to 7% higher than those determined at Rutgers.

A4.3 ICP-MS (MIT) Compared to INAA (MIT)

[66] In Figure A5, we also compare results obtained by ICP-MS and INAA for REE, Hf and Th. Except for Tb and Th the linear correlation coefficients between the results from ICP-MS and INAA are greater than 0.96. The poorer correlation for Tb and Th reflects the poorer precision of INAA data for these elements (see precision estimates in *Yang et al.* [1996, Table 1]). Also there is a systematic discrepancy between the two techniques for Tb, Yb and Lu. The INAA results are ~8% lower than the ICP-MS data; this same

Table A4. Input Parameters for Melting Model

	Mineral Proportions						Source Composition				
	Olivine	OPX	CPX	Sp	Grt		Nb/Zr	La/Sm	La/Yb	Sm/Yb	Ti/Zr
Source Mode[a]											
Grt Peridotite	0.53	0.04	0.33	0	0.1		0.076	1.9	1.8	0.9	80
Sp Peridotite	0.53	0.2	0.25	0.02	0	normalized to PM	1.20	1.20	1.22	1.02	0.72
Melting Reaction[a]											
Grt Peridotite	0.05	−0.49	1.31	0	0.13						
Sp Peridotite	0.375	−0.5	1.125	0	0						

Partition Coefficients

	OPX[b]			CPX			
	Grt Peridotite	Sp Peridotite	Olivine	Grt Peridotite[c]	Sp Peridotite[d]	Spinel	Garnet[c]
La	0.00001	0.00008	0	0.008[e]	0.045[e]	0	0.023[e]
Sm	0.00083	0.0038	0	0.07	0.319	0	0.318
Yb	0.02	0.0569	0	0.174	0.503	0	5.17
Nb	0.00022	0.0013	0	0.008	0.045	0	0.023
Zr	0.0013	0.0066	0	0.027	0.138	0	0.411
Ti	0.017	0.087	0	0.081[f]	0.414[f]	0	0.2/0.03[g]

[a] From Table 2 of *Salters* [1996].
[b] Calculated using $K_d^{OPX/CPX}$ values of sample 2905 from *Eggins et al.* [1998].
[c] From *Salters and Longhi* [1999], sample TM 694-6 (2.8GPa and 1537°C).
[d] From *Salters and Longhi* [1999], sample TM 1094-9 (1.5GPa and 1502°C).
[e] $Kd_{La}^{CPX/melt} = Kd_{Nb}^{CPX/melt}$ and $Kd_{La}^{Grt/melt} = Kd_{Nb}^{Grt/melt}$ are assumed.
[f] Since $(Ti/Zr)_{CPX}/(Ti/Zr)_{melt}$ is ~3 [*Hart and Dunn*, 1993; *Skulski et al.*, 1994; *Johnson*, 1998], $Kd_{Ti}^{CPX/melt} = 3Kd_{Zr}^{CPX/melt}$.
[g] Since $Kd_{Ti}^{Grt/CPX}$ ranges from 0.4 to 2 [Harte and Kirkley, 1997], two values are used for $Kd_{Ti}^{Grt/melt}$. In model "garnet peridotite a", $Kd_{Ti}^{Grt/melt}$ = 0.2; in model "garnet peridotite b", $Kd_{Ti}^{Grt/melt}$ = 0.03. These yield $(Ti/Zr)_{grt}/(Ti/Zr)_{melt}$ = 0.07 and 0.49; the latter value is similar to the ratio (0.3 to 0.7) found by *van Westrenen et al.* [1999].

discrepancy was found for analyses of BHVO-2 (Table A3).

Appendix B

[67] In order to evaluate the relationships between HSDP 2 lavas, we calculated La/Yb-Nb/Zr, Sm/Yb-Nb/Zr, Sm/Yb-La/Yb and La/Yb-Ti/Zr trends for variable extents of batch melting of garnet- and spinel- peridotite (Figure 10). Source abundances and mineral proportions and melting reactions are in Table A4. The partition coefficients are assumed to be zero for olivine/melt and spinel/melt. For clinopyroxene and garnet the partition coefficients vary with mineral composition and the values used are in Table A4. For garnet peridotite we used data for high pressure clinopyroxene and garnet (TM 694-6) from *Salters and Longhi* [1999]. For spinel peridotite we used data for a lower pressure clinopyroxene (TM 1094-9) from *Salters and Longhi* [1999]. For orthopyroxene, we estimated partition coefficients from measured $D^{opx/cpx}$ ratios [*Eggins et al.*, 1998]. For more detailed information, see the footnote of Table A4.

Acknowledgments

[68] We thank D. DePaolo, E. Stolper and D. Thomas for their leadership of the HSDP, M. Garcia, C. Seaman and the logging crew for their on site efforts, and our colleagues studying these cores who shared their data. We thank J. M. Rhodes for numerous discussions and an informal review. P. Ila is thanked for her supervision of the MIT neutron activation facility. A. Pietruszka, K. Sims, and H. Zou provided helpful constructive reviews. This research was supported by National Science Foundation Grant EAR-9528594. We thank M. Schmitz and B. Grant for their assistance in ICP-MS analysis.

References

Abouchami, W., S. J. G. Galer, and A. W. Hofmann, High precision lead isotope systematics of lavas from the Hawaiian Scientific Drilling Project, *Chem. Geol.*, *169*, 187–209, 2000.

Albarede, F., High-resolution geochemical stratigraphy of Mauna Kea flows from the Hawaii Scientific Drilling Project core, *J. Geophys. Res.*, *101*, 11,841–11,853, 1996.

Baker, M. B., S. Alves, and E. M. Stolper, Petrography and petrology of the Hawaii Scientific Drilling Project lavas: Inferences from olivine phenocryst abundances and compositions, *J. Geophys. Res.*, *101*, 11,715–11,727, 1996.

Blichert-Toft, J., F. A. Frey, and F. Albarède, Hf isotope evidence for pelagic sediments in the source of Hawaiian basalts, *Science*, *285*, 879–882, 1999.

Blundy, J. D., J. A. C. Robinson, and B. J. Wood, Heavy REE are compatible in clinopyroxene on the spinel lherzolite solidus, *Earth Planet. Sci. Lett.*, *160*, 493–504, 1998.

Chan, L.-H., and F. A. Frey, Lithium isotope geochemistry of the Hawaiian plume: Results from the Hawaii Scientific Drilling Project and Koolau Volcano, *Geochem. Geophys. Geosyst.*, *4*(3), 8707, doi:10.1029/2002GC000365, 2003.

Chauvel, C., and C. Hemond, Melting of a complete section of recycled oceanic crust: Trace element and Pb isotopic evidence from Iceland, *Geochem. Geophys. Geosyst.*, *1*, Paper number 1999GC000002, 2000.

Chen, C.-Y., F. A. Frey, M. O. Garcia, G. B. Dalrymple, and S. R. Hart, The tholeiitic to alkalic basalt transition at Haleakala volcano, Maui, Hawaii, *Contrib. Mineral. Petrol.*, *106*, 183–200, 1990.

Chen, C.-Y., F. A. Frey, M. O. Garcia, B. Dalrymple, and S. R. Hart, The tholeiite to alkalic basalt transition at Haleakala Volcano, Maui, Hawaii: Petrogenetic interpretations based on major and trace element and isotope geochemistry, *Contrib. Mineral. Petrol.*, *106*, 183–200, 1991.

Chen, C.-Y., F. A. Frey, J. M. Rhodes, and R. M. Easton, Temporal geochemical evolution of Kilauea Volcano: Comparison of Hilina and Puna Basalt, in *Earth Processes: Reading the Isotopic Code*, *Geophys. Monogr. Ser.*, vol. 95, edited by A. Basu and S. R. Hart, pp. 161–181, AGU, Washington, D.C., 1996.

Cohen, A. S., R. K. O'Nions, and M. D. Kurz, Chemical and isotopic variations in Mauna Loa tholeiites, *Earth Planet. Sci. Lett.*, *143*, 111–124, 1996.

David, K., P. Schiano, and C. J. Allegre, Assessment of the Zr/Hf fractionation in oceanic basalts and continental materials during petrogenetic processes, *Earth Planet. Sci. Lett.*, *178*, 285–301, 2000.

DePaolo, D. J., and E. M. Stolper, Models of Hawaiian volcano growth and plume structure; Implications of results from the Hawaii Scientific Drilling Project, *J. Geophys. Res.*, *101*, 11,643–11,654, 1996.

DePaolo, D. J., E. M. Stolper, D. M. Thomas, and M. O. Garcia, Hawaii Scientific Drilling Project: Core logs and summarizing data, rep, Calif. Inst. of Technol., Pasadena, 1999.

DePaolo, D. J., J. G. Bryce, A. Dodson, D. L. Shuster, and B. M. Kennedy, Isotopic evolution of Mauna Loa and the chemical structure of the Hawaiian plume, *Geochem. Geophys. Geosyst.*, *2*, Paper number 2000GC000139, 2001.

Eggins, S. M., R. L. Rudnick, and W. F. McDonough, The composition of peridotites and their minerals: A laser ablation ICP-MS study, *Earth Planet. Sci. Lett.*, *154*, 53–71, 1998.

Eiler, J. M., J. W. Valley, and E. M. Stolper, Oxygen isotope ratios in olivine from the Hawaii Scientific Drilling Project, *J. Geophys. Res.*, *101*, 11,807–11,813, 1996.

Feigenson, M. D., A. W. Hofmann, and F. J. Spera, Case studies on the origin of basalt, II, The transition from tholeiitic to alkalic volcanism on Kohala volcano, Hawaii, *Contrib. Mineral. Petrol.*, *84*, 390–405, 1983.

Frey, F. A., and D. A. Clague, Geochemistry of diverse basalt types from Loihi Seamount, Hawaii; petrogenetic implications, *Earth Planet. Sci. Lett.*, *66*, 337–355, 1983.

Frey, F. A., and J. M. Rhodes, Inter-shield geochemical differences among Hawaiian volcanoes: Implications for source compositions, melting processes and magma ascent paths, *Philos. Trans. R. Soc. London Ser. A.*, *342*, 121–136, 1993.

Frey, F. A., W. S. Wise, H. West, S. T. Kwon, and A. Kennedy, Evolution of Mauna Kea volcano, Hawaii: Petrologic and geochemical constraints on postshield volcanism, *J. Geophys. Res.*, *95*, 1271–1300, 1990.

Frey, F. A., M. O. Garcia, W. S. Wise, A. Kennedy, P. Gurriet, and F. Albarede, The evolution of Mauna Kea volcano, Hawaii: Petrogenesis of tholeiitic and alkalic basalts, *J. Geophys. Res.*, *96*, 14,347–14,375, 1991.

Garcia, M. O., B. A. Jorgenson, J. J. Mahoney, E. Ito, and A. J. Irving, An evaluation of temporal geochemical evolution of Loihii summit lavas: Results from Alvin submersible dives, *J. Geophys. Res.*, *98*, 535–550, 1993.

Garcia, M. O., D. J. P. Foss, H. B. West, and J. J. Mahoney, Geochemical and isotopic evolution of Loihi Volcano, Hawaii, *J. Petrol.*, *36*, 1644–1647, 1995.

Garcia, M. O., J. M. Rhodes, F. A. Trusdell, and A. Pietruszka, Petrology of lavas from Puu Oo eruption of Kilauea Volcano, III, The Pond Stage (1986–1992), *Bull. Volcanology*, *58*, 359–379, 1996.

Garcia, M. O., K. H. Rubin, M. D. Norman, J. M. Rhodes, D. W. Graham, D. W. Muenow, and K. Spencer, Petrology and geochronology of basalt breccia from the 1996 earthquake swarm of Loihi Seamount, Hawaii; Magmatic history of its 1996 eruption, *Bull. Volcanol.*, *59*, 577–592, 1998.

Green, D. H., T. Falloon, S. M. Eggins, and G. M. Yaxley, Primary magmas and mantle temperatures Anonymous, Experimental mineralogy, petrology and geochemistry, *Eur. J. Mineral.*, *13*, 437–451, 2001.

Hanson, G. N., An approach to trace element modeling using a simple igneous system as an example in geochemistry and mineralogy of rare earth elements, *Rev. Mineral.*, *21*, 79–97, 1989.

Hart, S. R., A large-scale isotope anomaly in the Southern Hemisphere mantle, *Nature*, *309*, 753–757, 1984.

Hart, S. R., and T. Dunn, Experimental clinopyroxene/melt partitioning for 24 trace elements, *Contrib. Mineral. Petrol.*, *113*, 108, 1993.

Hauri, E. H., Major-element variability in the Hawaiian mantle plume, *Nature*, *382*, 415–419, 1996.

Hofmann, A. W., Nb in Hawaiian magmas; Constraints on source composition and evolution, *Chem. Geol.*, *57*, 17–30, 1986.

Hofmann, A. W., Chemical differentiation of the earth: The relationship between mantle, continental crust, and oceanic crust, *Earth Planet. Sci. Lett.*, *90*, 297–314, 1988.

Hofmann, A. W., and K. P. Jochum, Source characteristics derived from very incompatible trace elements in Mauna Loa and Mauna Kea basalts (Hawaiian Scientific Drilling Project), *J. Geophys. Res.*, *101*, 11,831–11,839, 1996.

Hofmann, A. W., and W. M. White, Ba, Rb and Cs in the Earth's mantle, *Z. Naturforssch*, *38a*, 258–266, 1983.

Ila, P., and F. A. Frey, Utilization of neutron activation analysis in the study of geologic materials, in *Use and Development of Low and Medium Flux Research Reactors*, suppl. to vol. 44, edited by O. K. Harling, L. Clark, and P. von der Hardt, pp. 710–716, Atomkerenergie Kerntechnik, 1984.

Ila, P., and F. A. Frey, Trace element analysis of USGS standards AGV2, BCR2, GHVO2, DTS2 and GSP2 by INAA, *J. Radioanal. Nuclear Chem.*, *244*, 599–602, 2000.

Jackson, M. C., R. A. Wilmoth, and F. A. Frey, Geology and petrology of basaltic lavas and dikes of the Koolau Volcano in the Trans-Koolau exploratory tunnels, Oahu, Hawaii, *Bull. Volcan.*, *60*, 381–401, 1999.

Johnson, K. T. M., Experimental determination of partition coefficients for rare earth and high-field-strength elements between clinopyroxene, garnet, and basaltic melt at high pressures, *Contrib. Mineral. Petrol.*, *133*, 60–68, 1998.

Kamber, B. S., and K. D. Collerson, Zr/Nb systematics of ocean island basalts reassessed - The case for binary mixing, *J. Petrol.*, *41*, 1007–1021, 2000.

Kennedy, A. K., S. T. Kwon, F. A. Frey, and H. B. West, The isotopic composition of postshield lavas from Mauna Kea Volcano Hawaii, *Earth Planet. Sci. Lett.*, *103*, 339–353, 1991.

Kurz, M. D., and J. M. Curtice, Helium isotopic evolution of Mauna Kea Volcano: New results from the 3 Km drill core, *Eos Trans. AGU*, *81*(48), Fall Meet. Suppl., F1343, 2000.

Kurz, M. D., M. O. Garcia, F. A. Frey, and P. A. O'Brien, Temporal helium isotopic variations within Hawaiian volcanoes: Basalts from Mauna Loa and Haleakala, *Geochim. Cosmochim. Acta*, *51*, 2905–2914, 1987.

Kurz, M. D., T. C. Kenna, D. P. Kammer, J. M. Rhodes, and M. O. Garcia, Isotopic evolution of Mauna Loa volcano: A view from the submarine southwest rift Mauna Loa: A Decade Volcano, in *Mauna Loa Revealed*, *Geophys. Monogr. Ser.*, vol. 92, edited by J. M. Rhodes and J. P. Lockwood, pp. 289–306, AGU, Washington, D.C., 1995.

Kurz, M. D., T. C. Kenna, J. C. Lassiter, and D. J. DePaolo, Helium isotopic evolution of Mauna Kea volcano: First results from the 1-km drill core, *J. Geophys. Res.*, *101*, 11,781–11,791, 1996.

Lassiter, J. C., and E. H. Hauri, Osmium-iosotope variations in Hawaiian lavas: Evidence for recycled oceanic lithosphere in the Hawaiian plume, *Earth Planet. Sci. Lett.*, *164*, 483–496, 1998.

Lassiter, J. C., D. J. DePaolo, and M. Tatsumoto, Isotopic evolution of Mauna Kea volcano: Results from the initial phase of the Hawaiian Scientific Drilling Project, *J. Geophys. Res.*, *101*, 11,769–11,780, 1996.

Lin, S., M. He, H. Hu, H. Yuan, and S. Gas, Precise determination of trace elements in geological samples by ICP-MS using compromise conditions and fine matrix-matching strategy, *Anal. Sci.*, *16*, 1291–1296, 2000.

Moore, J. G., Density of basalt core from Hilo drill hole, Hawaii, *J. Volcanol. Geotherm. Res.*, *112*, 221–230, 2001.

Norman, M. D., and M. O. Garcia, Primitive magmas and source characteristics of the Hawaiian Plume; Petrology and geochemistry of shield picrites, *Earth Planet. Sci. Lett.*, *168*, 27–44, 1999.

Pietruszka, A. J., and M. O. Garcia, A rapid fluctuation in the mantle source and melting history of Kilauea Volcano inferred from the geochemistry of its historical summit lavas (1790–1982), *J. Petrol.*, *40*, 1321–1342, 1999.

Pietruszka, A. J., K. H. Rubin, and M. O. Garcia, $^{226}RA2^{30}$ Th-^{238}U disequilibria of historical Kilauea lavas (1790–1982) and the dynamics of mantle melting within the Hawaiian Plume, *Earth Planet. Sci. Lett.*, *186*, 15–31, 2001.

Raczek, I., B. Stoll, A. W. Hofmann, and K. P. Jochum, High precision trace element data for USGS reference materials BCR-1, BCR-2, BHVO-1, BHVO-2, AGU-1, AGU-2, DTS-1, DTS-2, GSP-1, and GSP-2 by ID-TIMS and MIC-SSMS, *Geostandards Newsl.*, *25*, 77–86, 2001.

Rhodes, J. M., The 1852 and 1868 Mauna Loa picrite eruptions: Clues to parental magma compositions and the magmatic plumbing system, in *Mauna Loa Revealed*, *Geophys. Monogr. Ser.*, vol. 92, edited by J. M. Rhodes and J. P. Lockwood, pp. 241–262, AGU, Washington, D.C., 1995.

Rhodes, J. M., Geochemical stratigraphy of lava flows sampled by the Hawaii Scientific Drilling Project, *J. Geophys. Res.*, *101*, 11,729–11,746, 1996.

Rhodes, J. M., Geochemistry of Mauna Loa and Mauna Kea Lavas sampled by the Hawaii Scientific Drilling Project, *Eos Trans. AGU*, *81*(48), Fall Meet. Suppl., F1342, 2000.

Rhodes, J. M., and S. R. Hart, Episodic trace element and isotopic variation in historical Mauna Loa lavas, in *Mauna Loa Revealed*, *Geophys. Monogr. Ser.*, vol. 92, edited by J. M. Rhodes and J. P. Lockwood, pp. 263–288, AGU, Washington, D.C., 1995.

Roden, M. F., T. Trull, S. R. Hart, and F. A. Frey, New He, Sr, Nd and Pb isotopic constraints on the constitution of the Hawaiian plume: Results from Koolau Volcano, Oahu, Hawaii, *Geochim. Cosmochim. Acta*, *58*, 1431–1440, 1994.

Salters, V. J. M., The generation of mid-ocean ridge basalts from the Hf and Nd isotope perspective, *Earth Planet. Sci. Lett.*, *141*, 109–123, 1996.

Salters, V. J. M., and J. Longhi, Trace element partitioning during the initial stages of melting beneath mid-ocean ridges, *Earth Planet. Sci. Lett.*, *166*, 15–30, 1999.

Sharp, W., B. Turrin, P. Renne, and M. Lanphere, The ^{40}Ar/^{39}Ar and K/Ar dating of lavas from the Hilo 1-km core hold, Hawaiian Scientific Drilling Project, *J. Geophys. Res.*, *101*, 11,604–11,616, 1996.

Skulski, T., W. Minarik, and E. B. Watson, High pressure experimental trace-element partitioning between clinopyroxene and basaltic melts, *Chem. Geol.*, *117*, 127–147, 1994.

Sobolev, A. V., A. W. Hofmann, and I. K. Nikogosian, Recycled oceanic crust observed in ghost plagioclase within the source of Mauna Loa lavas, *Nature*, *404*, 986–990, 2000.

Staudigel, H., G. R. Davies, S. R. Hart, K. M. Marchant, and B. M. Smith, Large scale isotopic Sr, Nd and O isotopic anatomy of altered oceanic crust: DSDP/ODP sites 417/418, *Earth Planet. Sci. Lett.*, *130*, 169–185, 1995.

Stolper, E., and M. Baker (Eds.), *Hawaii Scientific Drilling Project, Core-Logs*, 471 pp., Calif. Inst. of Tech., Pasadena, 1994.

Stolper, EM., D. J. DePaolo, and D. M. Thomas, Introduction to special section: Hawaii Scientific Drilling Project, *J. Geophys. Res.*, *101*, 11,593–11,598, 1996.

Sun, S.-S., and W. F. McDonough, Chemical and isotopic systematics of oceanic basalts: Implications for mantle composition and processes, in *Magmatism in the Ocean Basins*, edited by A. D. Saunders and M. J. Norry, *Geol. Soc. Spec. Publ., 42*, 313–345, 1989.

van Westrenen, W., J. Blundy, and B. Wood, Crystal-chemical controls on trace element partitioning between garnet and anhydrous silicate melt, *Am. Mineral.*, *84*, 838–847, 1999.

Wolfe, E. W., W. S. Wise, and G. B. Dalrymple, The geology and petrology of Mauna Kea Volcano, Hawaii; a study of postshield volcanism, *U. S. Geol. Surv. Prof. Pap.*, *1557*, 1–129, 1997.

Yang, H.-J., F. A. Frey, M. O. Garcia, and D. A. Clague, Submarine lavas from Mauna Kea volcano, Hawaii: Implications for Hawaiian shield-stage processes, *J. Geophys. Res.*, *99*, 15,577–15,594, 1994.

Yang, H.-J., F. A. Frey, J. M. Rhodes, and M. O. Garcia, Evolution of Mauna Kea volcano: Inferences from lava compositions recovered in the Hawaii Scientific Drilling Project, *J. Geophys. Res.*, *101*, 11,747–11,767, 1996.

Yang, H.-J., F. A. Frey, and D. A. Clague, Constraints on the source components of lavas forming the Hawaiian North Arch and Honolulu Volcanoes, *J. Petrol.*, *44*, 603–627, 2003.